

Importance sampling for a robust and efficient multilevel Monte Carlo estimator for stochastic reaction networks

Chiheb Ben Hammouda* Nadhir Ben Rached † Raúl Tempone‡§

Abstract

The multilevel Monte Carlo (MLMC) method for continuous time Markov chains, first introduced by Anderson and Higham [3], is a highly efficient simulation technique that can be used to estimate various statistical quantities for stochastic reaction networks (SRNs), and in particular for stochastic biological systems. Unfortunately, the robustness and performance of the multilevel method can be deteriorated due to the phenomenon of high kurtosis, observed at the deep levels of MLMC, which leads to inaccurate estimates for the sample variance. In this work, we address cases where the high-kurtosis phenomenon is due to *catastrophic coupling* (characteristic of pure jump processes where coupled consecutive paths are identical in most of the simulations, while differences only appear in a very small proportion), and introduce a pathwise dependent importance sampling technique that improves the robustness and efficiency of the multilevel method. Our analysis, along with the conducted numerical experiments, demonstrates that our proposed method significantly reduces the kurtosis of the deep levels of MLMC, and also improves the strong convergence rate from $\beta = 1$ for the standard case (without importance sampling), to $\beta = 1 + \delta$, where $0 < \delta < 1$ is a user-selected parameter in our importance sampling algorithm. Due to the complexity theorem of MLMC and given a pre-selected tolerance, TOL , this results in an improvement of the complexity from $\mathcal{O}(TOL^{-2} \log(TOL)^2)$ in the standard case to $\mathcal{O}(TOL^{-2})$.

Keywords Multilevel Monte Carlo. Continuous time Markov chains. Stochastic reaction networks. Stochastic biological systems. Importance sampling.

2010 Mathematics Subject Classification 60H35. 60J27. 60J75. 92C40.

1 Introduction

In this work, we propose a novel importance sampling algorithm that can be combined with the multilevel Monte Carlo (MLMC) estimator to numerically solve stochastic differential equations (SDEs) driven by Poisson random measures [24, 9].

*King Abdullah University of Science and Technology (KAUST), Computer, Electrical and Mathematical Sciences & Engineering Division (CEMSE), Thuwal 23955 – 6900, Saudi Arabia (chiheb.benhammouda@kaust.edu.sa).

†Chair of Mathematics for Uncertainty Quantification, RWTH Aachen University, Aachen 52072, Germany. (benrached@uq.rwth-aachen.de).

‡King Abdullah University of Science and Technology (KAUST), Computer, Electrical and Mathematical Sciences & Engineering Division (CEMSE), Thuwal 23955 – 6900, Saudi Arabia (raul.tempone@kaust.edu.sa).

§Alexander von Humboldt Professor in Mathematics for Uncertainty Quantification, RWTH Aachen University, Aachen 52072, Germany.

We focus on a particular class of continuous-time Markov chains known as stochastic reaction networks (SRNs) (see Section 1.1 for a short introduction). SRNs describe the time evolution of biochemical reactions, epidemic processes [7, 5], and transcription and translation in genomics and virus kinetics [30, 20], among other important applications.

Let \mathbf{X} be an SRN taking values in \mathbb{Z}_+^d and defined in the time-interval $[0, T]$, where $T > 0$ is a user-selected final time. We aim to provide accurate MLMC estimations of the expected value, $E[g(\mathbf{X}(T))]$, where $g : \mathbb{R}^d \rightarrow \mathbb{R}$ is a given smooth scalar observable of \mathbf{X} .

The main goal of our new proposed method is to increase the robustness (we consider as a robust estimator, an estimator that is not unduly affected by the presence of outliers¹) and performance of the MLMC estimator by i) solving the high-kurtosis phenomenon encountered when using the multilevel method in the context of continuous-time Markov chains (see Section 1.4), and ii) lowering the complexity of the MLMC estimator by reducing the variance of the MLMC levels and even increasing their strong convergence rate.

Many methods have been developed to simulate exact sample paths of SRNs; for instance, the stochastic simulation algorithm (SSA) was introduced by Gillespie in [16] and the modified next reaction method (MNRM) was proposed by Anderson in [4]. Pathwise exact realizations of SRNs may be computationally very costly when some reaction channels have high reaction rates. To overcome this issue, Gillespie [17] and Aparicio and Solari [6] independently proposed the explicit tau-leap (TL) method (see Section 1.2) to simulate approximate paths of \mathbf{X} by evolving the process with fixed time steps, keeping the reaction rates fixed within each time step. Furthermore, other simulation schemes have been proposed to deal with situations with well-separated fast and slow time scales [8, 29, 1, 2, 25, 19].

To reduce the computational work needed to compute an estimate of $E[g(\mathbf{X}(T))]$, Anderson and Higham [3] introduced the MLMC method [14, 15] based on the explicit TL scheme in the context of SRNs. Many extensions of the MLMC method have since been introduced to address other challenges in this context. For instance, adaptive multilevel estimators [23, 26, 25] were proposed to improve the performance of non-adaptive estimators [3] to simulate SRNs with markedly different time scales. Furthermore, [19] extended [3] to systems with slow and fast time scales, and introduced a hybrid multilevel estimator that uses an implicit scheme for levels where explicit TL can not be used due to numerical instability.

One important challenge encountered when using MLMC in the context of SRNs is the high-kurtosis phenomenon (result of infrequent extreme deviations; see Section 1.4 for more details), which may occur due to either *catastrophic coupling* (characteristic of pure jump processes where coupled consecutive paths are identical in most of the simulations, while differences only appear in a very small proportion; see Section 1.4.1 for more details) or *catastrophic decoupling* (observed for general stochastic processes where terminal values of the sample paths of both coarse and fine levels become very different from each other; see Section 1.4.2 for more details). This bad behavior of kurtosis affects the accurate estimation of the sample variance needed for the MLMC algorithm, and consequently it affects the robustness and performance of the multilevel estimator in many cases. Only a few works have addressed this issue to date; for instance, the authors in [26] mentioned this issue and developed a more accurate estimator for the multilevel variance based on dual-weighted residual expansion techniques. In [22], a new method has been proposed to address the high-kurtosis phenomenon when it is due to *catastrophic decoupling*, and introduced a new

¹infrequent extreme deviations

way of coupling consecutive levels of MLMC called the *common process method* (CPM), instead of using the *split propensity method* (SPM) proposed in [3]. The CPM is based on the use of common inhomogeneous Poisson processes for both coarse and fine samples paths. Although the CPM increases the robustness and reliability of the multilevel estimator by dramatically decreasing the kurtosis, it nonetheless incurs remarkable additional computational and memory costs since for each level it requires i) running the TL algorithm twice, and ii) storing the total number of times each Poisson process has fired over each time step.

In our work, in contrast to [22], we address cases of high kurtosis observed in the MLMC estimator due to *catastrophic coupling* and propose a novel method that provides a more robust multilevel estimator (our estimator is resistant to the high kurtosis, which is a result of the presence of outliers). We introduce a pathwise dependent importance sampling technique to dramatically decrease the high kurtosis caused by the SPM strategy for coupling the paths of two consecutive levels. In this work, we show that our proposed method not only increases the robustness of the multilevel estimator by significantly reducing the kurtosis, but also improves the strong convergence rate from $\beta = 1$ for the standard case (without importance sampling), to $\beta = 1 + \delta$, where $0 < \delta < 1$ is a user-selected parameter in our importance sampling algorithm. Due to the complexity theorem of MLMC, and given a pre-selected tolerance, TOL , this results in improving the complexity of MLMC from $\mathcal{O}(TOL^{-2} \log(TOL)^2)$ in the standard case to $\mathcal{O}(TOL^{-2})$ (see Figure 3.1).

Alternatively, a complexity of order $\mathcal{O}(TOL^{-2})$ can be achieved by using i) MC with an exact scheme (for instance SSA), or ii) an unbiased MLMC estimator [3], where the finest level is simulated with an exact scheme, or iii) a biased hybrid MLMC estimator [26], where the paths are simulated in a hybrid fashion that switches adaptively, based on the relative computational cost, between the TL and an exact method. Both i) and ii) above incur a huge additional cost by introducing an exact scheme. This remarkable additional cost is not manifested in the rate exponent but in a large constant that deteriorates the actual complexity. Although our method is based on a biased MLMC estimator, without steps simulated with an exact scheme as in [26], it still achieves a complexity of order $\mathcal{O}(TOL^{-2})$ with a smaller constant than those produced by the aforementioned ways (i), ii) and iii) above). In contrast to [3], we suggest an orthogonal way of lowering the complexity rate by improving the strong convergence rate, instead of removing the bias (weak error). Similarly to our work, the authors in [26] improve the strong convergence rate to reach the complexity of order $\mathcal{O}(TOL^{-2})$. However, compared to [26], we use a different strategy based on a pathwise dependent importance sampling coupled with the TL scheme, instead of using a hybrid approach that switches between an exact and the TL scheme as in [26].

We also propose a new way to overcome the high-kurtosis phenomenon, which affects the robustness and reliability of the MLMC estimator introduced in [3]. Although this issue can be addressed differently by using the dual-weighted residual expansion techniques developed in [26] to estimate more accurately the sample variance and bias on the deepest levels of MLMC, we think that our approach has two main advantages over the approach in [26]: first, our method is much simpler and is easier to generalize to other schemes, such as the split step implicit TL scheme [19], where it is difficult to get estimates using the dual-weighted residual expansion techniques. Furthermore, although the approach in [26] provides a more accurate estimate for the variance than the sample variance estimates, there is still no clear analysis of how accurate (biased) those estimates are. This is mainly because of the lack of sharp concentration inequalities for linear combinations of independent Poisson random variables, as stated in Remark 4 in [26].

The outline of this paper is as follows: we start by giving an overview of concepts used in

this work such as SRNs (Section 1.1), explicit TL approximation (Section 1.2), and the MLMC method (Section 1.3). Then, in Section 1.4, we explain the high-kurtosis phenomenon along with its main causes in the context of SRNs. In Section 2, we present the details of our importance sampling algorithm that we combine with the MLMC method. We start by presenting in Section 2.1 the motivation of our idea by the sampling under a near optimal measure for simulating SRNs. Then, in Section 2.2, we present and analyze our proposed importance sampling algorithm. Before concluding, in Section 3 we show the results obtained through the numerical experiments conducted across different examples of SRNs.

1.1 Stochastic Reaction Networks (SRNs)

We are interested in the time evolution of a homogeneously mixed chemical reacting system described by the Markovian pure jump process, $\mathbf{X} : [0, T] \times \Omega \rightarrow \mathbb{Z}_+^d$, where (Ω, \mathcal{F}, P) is a probability space. In this framework, we assume that d different species interact through J reaction channels. The i -th component, $X^{(i)}(t)$, describes the abundance of the i -th species present in the chemical system at time t . The aim of this work is to study the time evolution of the state vector,

$$\mathbf{X}(t) = (X^{(1)}(t), \dots, X^{(d)}(t)) \in \mathbb{Z}_+^d.$$

Each reaction channel, \mathcal{R}_j , is a pair $(a_j, \boldsymbol{\nu}_j)$, defined by its propensity function, $a_j : \mathbb{R}^d \rightarrow \mathbb{R}_+$, and its state change vector, $\boldsymbol{\nu}_j = (\nu_{j,1}, \nu_{j,2}, \dots, \nu_{j,d})$, satisfying²

$$(1.1) \quad \text{Prob}(\mathbf{X}(t + \Delta t) = \mathbf{x} + \boldsymbol{\nu}_j; \mathbf{X}(t) = \mathbf{x}) = a_j(\mathbf{x})\Delta t + o(\Delta t), \quad j = 1, 2, \dots, J.$$

Formula (1.1) states that the probability of observing a jump in the process, \mathbf{X} , from state \mathbf{x} to state $\mathbf{x} + \boldsymbol{\nu}_j$, a consequence of the firing of reaction \mathcal{R}_j , during a small time interval, $(t, t + \Delta t]$, is proportional to the length of the time interval, Δt , with $a_j(\mathbf{x})$ as the constant of proportionality.

We set $a_j(\mathbf{x})=0$ for those \mathbf{x} such that $\mathbf{x} + \boldsymbol{\nu}_j \notin \mathbb{Z}_+^d$ (*the non-negativity assumption*: the system can never produce negative population values).

As a consequence of relation (1.1), the process \mathbf{X} is a continuous-time, discrete-space Markov chain that can be characterized by the random time change representation of Kurtz [13]

$$(1.2) \quad \mathbf{X}(t) = \mathbf{x}_0 + \sum_{j=1}^J Y_j \left(\int_0^t a_j(\mathbf{X}(s)) ds \right) \boldsymbol{\nu}_j,$$

where $Y_j : \mathbb{R}_+ \times \Omega \rightarrow \mathbb{Z}_+$ are independent unit-rate Poisson processes. Conditions on the reaction channels can be imposed to ensure uniqueness [5] and to avoid explosions in finite time [12, 28, 18]

1.2 The Explicit Tau-Leap (Explicit-TL) Approximation

The explicit-TL scheme is a pathwise-approximate method independently introduced in [17] and [6] to overcome the computational drawback of exact methods, *i.e.*, when many reactions fire during a short time interval. This scheme can be derived from the random time change representation of Kurtz (1.2) by approximating the integral $\int_{t_i}^{t_{i+1}} a_j(\mathbf{X}(s)) ds$ by $a_j(\mathbf{X}(t_i))(t_{i+1} - t_i)$,

²Hereafter, we use $\text{Prob}(A; B)$, $E[A; B]$, and $\text{Var}[A; B]$ to denote the conditional probability, conditional expectation, and conditional variance of A given B , respectively.

i.e., using the forward-Euler method with a time mesh $\{t_0 = 0, t_1, \dots, t_N = T\}$. In this way, the explicit-TL approximation of \mathbf{X} should satisfy for $k \in \{1, 2, \dots, N\}$

$$\mathbf{Z}(t_k) = \mathbf{x}_0 + \sum_{j=1}^J Y_j \left(\sum_{i=0}^{k-1} a_j(\mathbf{Z}(t_i))(t_{i+1} - t_i) \right) \boldsymbol{\nu}_j.$$

Given a uniform time mesh of size τ , we simulate a path of \mathbf{Z} as follows. Let $\mathbf{Z}(t_0) := \mathbf{x}_0$ and define

$$\mathbf{Z}(t_k) := \mathbf{z} + \sum_{j=1}^J \mathcal{P}_j(a_j(\mathbf{z})\tau) \boldsymbol{\nu}_j,$$

iteratively, where $\mathbf{z} = \mathbf{Z}(t_{k-1})$ and $\mathcal{P}_j(r_j)$ are independent Poisson random variables (rdvs) with respective rates, r_j . Notice that the explicit-TL path, \mathbf{Z} , is defined only at the points of the time mesh, but it can be naturally extended to $[0, T]$ as a piecewise constant path by defining $\mathbf{Z}(t_{k-1} + h) := \mathbf{Z}(t_{k-1}), \forall 0 < h < \tau$.

1.3 The Multilevel Monte Carlo (MLMC) Method

Let \mathbf{X} be a stochastic process and $g : \mathbb{R}^d \rightarrow \mathbb{R}$ a smooth scalar observable. Let us assume that we want to approximate $\mathbb{E}[g(\mathbf{X}(T))]$, but instead of sampling directly from $\mathbf{X}(T)$, we sample from $\mathbf{Z}_h(T)$, which are rdvs generated by an approximate method with step size h . Let us assume also that the variates $\mathbf{Z}_h(T)$ are generated with an algorithm with weak order, $\mathcal{O}(h)$, *i.e.*, $\mathbb{E}[g(\mathbf{X}(T)) - g(\mathbf{Z}_h(T))] = \mathcal{O}(h)$.

Let μ_M be the standard Monte Carlo estimator of $\mathbb{E}[g(\mathbf{Z}_h(T))]$ defined by

$$\mu_M := \frac{1}{M} \sum_{m=1}^M f(\mathbf{Z}_{h,[m]}(T)),$$

where $\mathbf{Z}_{h,[m]}(T)$ are independent and distributed as $\mathbf{Z}_h(T)$.

Consider now the following decomposition of the global error

$$\mathbb{E}[g(\mathbf{X}(T))] - \mu_M = (\mathbb{E}[g(\mathbf{X}(T)) - g(\mathbf{Z}_h(T))]) + (\mathbb{E}[g(\mathbf{Z}_h(T))] - \mu_M).$$

To achieve the desired accuracy, TOL , it is sufficient to take $h = \mathcal{O}(TOL)$ so that the first term on the right is $\mathcal{O}(TOL)$ and, by the Central Limit Theorem, impose $M = \mathcal{O}(TOL^{-2})$ so that the statistical error given by the second term on the right is $\mathcal{O}(TOL)$ [11]. As a consequence, the expected total computational work is $\mathcal{O}(TOL^{-3})$.

The MLMC estimator, introduced by Giles [14], allows us to reduce the total computational work. The basic idea of MLMC is to generate, and couple in an intelligent manner, paths with different step sizes, which results in

- i) Stochastically coordinated sequences of paths having different step sizes, where the paths with large step sizes are computationally less expensive than those with very small step sizes.
- ii) A small variance of the difference between two coupled paths with fine step sizes, implying significantly fewer samples in the estimation.

We can construct the MLMC estimator as follows: consider a hierarchy of nested meshes of the time interval $[0, T]$, indexed by $\ell = 0, 1, \dots, L$. We denote by h_0 the step size used at level $\ell = 0$. The size of the subsequent time steps for levels $\ell \geq 1$ are given by $h_\ell = K^{-\ell}h_0$, where $K > 1$ is a given integer constant. In this work, we take $K = 2$. To simplify the notation, hereafter \mathbf{Z}_ℓ denotes the approximate process generated using a step size of h_ℓ .

Consider now the following telescoping decomposition of $\mathbb{E}[g(\mathbf{Z}_L(T))]$

$$(1.3) \quad \mathbb{E}[g(\mathbf{Z}_L(T))] = \mathbb{E}[g(\mathbf{Z}_0(T))] + \sum_{\ell=1}^L \mathbb{E}[g(\mathbf{Z}_\ell(T)) - g(\mathbf{Z}_{\ell-1}(T))].$$

Then, by defining

$$\begin{cases} \widehat{Q}_0 := \frac{1}{M_0} \sum_{m_0=1}^{M_0} g(\mathbf{Z}_{0,[m_0]}(T)) \\ \widehat{Q}_\ell := \frac{1}{M_\ell} \sum_{m_\ell=1}^{M_\ell} (g(\mathbf{Z}_{\ell,[m_\ell]}(T)) - g(\mathbf{Z}_{\ell-1,[m_\ell]}(T))), \end{cases}$$

we arrive at the unbiased MLMC estimator, \widehat{Q} , of $\mathbb{E}[g(\mathbf{Z}_L(T))]$

$$\widehat{Q} := \sum_{\ell=0}^L \widehat{Q}_\ell.$$

We note that the key point here is that both $\mathbf{Z}_{\ell,[m_\ell]}(T)$ and $\mathbf{Z}_{\ell-1,[m_\ell]}(T)$ are sampled using different time discretizations but with the same generated randomness.

The following Theorem 1.1 from [10] demonstrates the computational complexity of the MLMC estimator for different scenarios.

Theorem 1.1. *Let g denote a random variable, and let g_ℓ denote the corresponding level ℓ numerical approximation.*

If there exist independent estimators Y_ℓ based on M_ℓ Monte Carlo samples, each with expected cost C_ℓ and variance V_ℓ , and positive constants α (weak convergence rate), β (strong convergence rate), γ (work rate), c_1, c_2, c_3 such that $\alpha \geq \min(\beta, \gamma)$ and

$$i) \quad |\mathbb{E}[g_\ell - g]| \leq c_1 2^{-\alpha\ell}$$

$$ii) \quad \mathbb{E}[Y_\ell] = \begin{cases} \mathbb{E}[g_0], & \ell = 0 \\ \mathbb{E}[g_\ell - g_{\ell-1}], & \ell > 0 \end{cases}$$

$$iii) \quad V_\ell \leq c_2 2^{-\beta\ell}$$

$$iv) \quad C_\ell \leq c_3 2^{\gamma\ell},$$

then there exists a positive constant c_4 such that for any $TOL < e^{-1}$, there are values L and M_ℓ for which the multilevel estimator

$$Y = \sum_{\ell=0}^L Y_\ell,$$

has a mean-square-error with bound

$$\mathbb{E} \left[(Y - \mathbb{E}[g])^2 \right] < TOL^2,$$

with a computational complexity C with bound

$$\mathbb{E}[C] = \begin{cases} c_4 TOL^{-2}, & \beta > \gamma, \\ c_4 TOL^{-2} (\log(TOL))^2, & \beta = \gamma, \\ c_4 TOL^{-2 - \frac{\gamma - \beta}{\alpha}}, & \beta < \gamma. \end{cases}$$

1.4 The high-kurtosis phenomenon

Let g denote a random variable, and let g_ℓ denote the corresponding level ℓ numerical approximation. We also define $Y_\ell = g_\ell - g_{\ell-1}$. The standard deviation of the sample variance for the random variable Y_ℓ is given by

$$(1.4) \quad \sigma_{S^2(Y_\ell)} = \frac{\text{Var}[Y_\ell]}{\sqrt{M}} \sqrt{(\kappa - 1) + \frac{2}{M - 1}},$$

where the kurtosis $\kappa = \frac{\mathbb{E}[(Y_\ell - \mathbb{E}[Y_\ell])^4]}{(\text{Var}[Y_\ell])^2}$.

Hence, $\mathcal{O}(\kappa)$ samples are required to obtain a reasonable estimate for the variance.

For the setting of the MLMC method, accurate estimates for $V_\ell = \text{Var}[Y_\ell]$ are required. Therefore, when the kurtosis of Y_ℓ is high, it affects both the robustness (no reliable estimates of the sample variance, V_ℓ) and also the performance (too many samples are required to control $\sigma_{S^2(Y_\ell)}$ given by (1.4)) of the multilevel estimator.

In the context of SRNs, the high-kurtosis phenomenon may be encountered when using the MLMC estimator, which deteriorates the robustness and the performance of the method. There are mainly two causes of the high-kurtosis phenomenon i) *Catastrophic coupling* or ii) *Catastrophic decoupling*. In the following subsections, we explain these two causes.

1.4.1 Catastrophic coupling

The high-kurtosis phenomenon in this case is caused by *catastrophic coupling* (see Section 1.7 of [26]), which is a characteristic of pure jump processes that motivates this work. When using the MLMC estimator in this context, the following issue is usually encountered: When ℓ (MLMC level) becomes large, due to the used coupling strategy (see Section 2.1), Y_ℓ is different from zero only in a very small proportion of the simulated coupled paths (see Figures 3.3, 3.9 3.14). This is one of the main causes of the high-kurtosis phenomenon (see Figures 3.2, 3.8 and 3.13), resulting in inaccurate estimates for the sample variance (see (1.4)). In this work, we address this issue by proposing a novel path-dependent importance sampling algorithm for the MLMC estimator.

As an illustration of *catastrophic coupling*, consider an example when g takes values in $\{0, 1\}$. In this case, we have

$$Y_\ell = g_\ell - g_{\ell-1} = \begin{cases} 1, & \text{with probability } p_\ell \\ -1, & \text{with probability } q_\ell \\ 0, & \text{with probability } 1 - p_\ell - q_\ell. \end{cases}$$

If $p_\ell, q_\ell \ll 1$, then $E[Y_\ell] \approx 0$ and $\kappa_\ell \approx (p_\ell + q_\ell)^{-1} \gg 1$. Therefore, many samples are required for a good estimate of $V_\ell = \text{Var}[Y_\ell]$; otherwise, we may get all samples $Y_\ell = 0$, which will give an estimated variance of zero. Furthermore, the kurtosis will become worse as $\ell \rightarrow \infty$ since $p_\ell, q_\ell \rightarrow 0$ due to weak convergence.

1.4.2 Catastrophic decoupling

The high-kurtosis phenomenon can also occur due to *catastrophic decoupling*, as explained in [21] and observed in [22]. *Catastrophic decoupling* occurs when the terminal values of the sample paths of both coarse and fine levels become very different from each other. In fact, due to the SPM coupling strategy (see Section 2.1), all reactions start immediately in the fine level and not in the coarse system, since reactions can not happen until the reaction propensities are updated. We note that this issue becomes more severe when dealing with large scales of species count.

We emphasize that we do not treat *catastrophic decoupling* with our novel proposed method, but rather the case of *catastrophic coupling* only (see Section 1.4.1). Nonetheless, the *catastrophic decoupling* can be addressed by using a different coupling, such as CPM coupling [22]. In a future work, to address the issue of *catastrophic decoupling*, we intend to explore the possibility of introducing a new importance sampling scheme for MLMC based on SPM coupling.

2 The construction of the importance sampling algorithm

2.1 Sampling under a near optimal measure

Let us use the notations of Section 1.3, and denote $g(\mathbf{Z}_\ell(T)) := g_\ell$. Then we can rewrite (1.3) as

$$(2.1) \quad E[g_L] = \sum_{\ell=1}^L E[g_\ell - g_{\ell-1}] + E[g_0],$$

where each term in (2.1) can be written as

$$E[g_0] = \int g_0 d\mathbb{P}_0, \quad E[g_\ell - g_{\ell-1}] = \int (g_\ell - g_{\ell-1}) d\mathbb{P}_\ell,$$

where \mathbb{P}_ℓ is the coupling measure.

In order to sample optimally, our sample measure should be

$$d\pi_0 \propto |g_0| d\mathbb{P}_0, \quad d\pi_\ell \propto |g_\ell - g_{\ell-1}| d\mathbb{P}_\ell.$$

Let us focus on the context of SRNs, and define the pure jump process X by the Kurtz representation as in (1.2). For the sake of simplicity, let us consider X to be one dimensional (only one species), only one reaction ($J = 1$) (in this case we denote the state change scalar by ν_1 ; see (1.1)), and $g(x) = x$, $x \in \mathbb{R}$. We denote $\bar{X}_{\ell-1}, \bar{X}_\ell$ the two TL approximations of the true process X based on two consecutive grid levels ($\ell - 1, \ell$). If we consider two consecutive time-mesh points for $\bar{X}_{\ell-1}$, $\{t_n, t_{n+1}\}$, and three consecutive time-mesh points for \bar{X}_ℓ , $\{t_n, t_n + \Delta t_\ell, t_{n+1}\}$, then we have

$$(2.2) \quad \begin{aligned} \bar{X}_{\ell-1}(t_{n+1}) &= \bar{X}_{\ell-1}(t_n) + \nu_1 \mathcal{Y}_{1,n} (a(\bar{X}_{\ell-1}(t_n)) \Delta t_{\ell-1}) \\ \bar{X}_\ell(t_n + \Delta t_\ell) &= \bar{X}_\ell(t_n) + \nu_1 \mathcal{Q}_{1,n} (a(\bar{X}_\ell(t_n)) \Delta t_\ell) \\ \bar{X}_\ell(t_{n+1}) &= \bar{X}_\ell(t_n + \Delta t_\ell) + \nu_1 \mathcal{R}_{1,n} (a(\bar{X}_\ell(t_n + \Delta t_\ell)) \Delta t_\ell), \end{aligned}$$

where $\mathcal{Y}_{1,n}, \mathcal{Q}_{1,n}, \mathcal{R}_{1,n}$ are independent Poisson rdvs.

To couple the $\bar{X}_{\ell-1}$ and \bar{X}_ℓ processes, we first decompose $\mathcal{Y}_{1,n}(a(\bar{X}_{\ell-1}(t_n))\Delta t_{\ell-1})$ as the sum of two independent Poisson rdvs, $\mathcal{P}_{1,n}(a(\bar{X}_{\ell-1}(t_n))\Delta t_\ell) + \mathcal{P}_{2,n}(a(\bar{X}_{\ell-1}(t_n))\Delta t_\ell)$. Then by applying this decomposition in (2.2), we obtain

$$\begin{aligned}\bar{X}_{\ell-1}(t_{n+1}) &= \bar{X}_{\ell-1}(t_n) + \nu_1 \mathcal{P}_{1,n}(a(\bar{X}_{\ell-1}(t_n))\Delta t_\ell) + \nu_1 \mathcal{P}_{2,n}(a(\bar{X}_{\ell-1}(t_n))\Delta t_\ell) \\ \bar{X}_\ell(t_{n+1}) &= \bar{X}_\ell(t_n) + \nu_1 \mathcal{Q}_{1,n}(a(\bar{X}_\ell(t_n))\Delta t_\ell) + \nu_1 \mathcal{R}_{1,n}(a(\bar{X}_\ell(t_n + \Delta t_\ell))\Delta t_\ell).\end{aligned}$$

Furthermore, using the same reasoning of coupling strategy as in [3], we can show that for the first time interval $[t_n, t_n + \Delta t_\ell]$, we have

$$(2.3) \quad \begin{aligned}\bar{X}_{\ell-1}(t_n + \Delta t_\ell) &= \bar{X}_{\ell-1}(t_n) + \left(\mathcal{P}'_n(m_{\ell,n}^1 \Delta t_\ell) + \mathcal{P}''_n((a(\bar{X}_{\ell-1}(t_n)) - m_{\ell,n}^1) \Delta t_\ell) \right) \nu_1 \\ \bar{X}_\ell(t_n + \Delta t_\ell) &= \bar{X}_\ell(t_n) + \left(\mathcal{P}'_n(m_{\ell,n}^1 \Delta t_\ell) + \mathcal{P}'''_n((a(\bar{X}_\ell(t_n)) - m_{\ell,n}^1) \Delta t_\ell) \right) \nu_1,\end{aligned}$$

where $m_{\ell,n}^1 = \min(a(\bar{X}_\ell(t_n)), a(\bar{X}_{\ell-1}(t_n)))$, and $\mathcal{P}'_n, \mathcal{P}''_n, \mathcal{P}'''_n$ are independent Poisson rdvs.

For the time interval $[t_n + \Delta t_\ell, t_{n+1}]$, we have

$$(2.4) \quad \begin{aligned}\bar{X}_{\ell-1}(t_{n+1}) &= \bar{X}_{\ell-1}(t_n + \Delta t_\ell) + \left(\mathcal{Q}'_n(m_{\ell,n}^2 \Delta t_\ell) + \mathcal{Q}''_n((a(\bar{X}_{\ell-1}(t_n)) - m_{\ell,n}^2) \Delta t_\ell) \right) \nu_1 \\ \bar{X}_\ell(t_{n+1}) &= \bar{X}_\ell(t_n + \Delta t_\ell) + \left(\mathcal{Q}'_n(m_{\ell,n}^2 \Delta t_\ell) + \mathcal{Q}'''_n((a(\bar{X}_\ell(t_n + \Delta t_\ell)) - m_{\ell,n}^2) \Delta t_\ell) \right) \nu_1,\end{aligned}$$

where $m_{\ell,n}^2 = \min(a(\bar{X}_\ell(t_n + \Delta t_\ell)), a(\bar{X}_{\ell-1}(t_n)))$, and $\mathcal{Q}'_n, \mathcal{Q}''_n, \mathcal{Q}'''_n$ are independent Poisson rdvs. (2.3) and (2.4) imply that

$$(2.5) \quad \begin{aligned}\bar{X}_\ell(t_{n+1}) - \bar{X}_{\ell-1}(t_{n+1}) &= \bar{X}_\ell(t_n) - \bar{X}_{\ell-1}(t_n) \\ &\quad + \nu_1 \left(\mathcal{P}'''_n(\Delta a_{\ell,n}^1 \Delta t_\ell) \mathbf{1}_{\Delta a_{\ell,n}^1 > 0} - \mathcal{P}''_n(-\Delta a_{\ell,n}^1 \Delta t_\ell) \mathbf{1}_{\Delta a_{\ell,n}^1 < 0} \right) \\ &\quad + \nu_1 \left(\mathcal{Q}'''_n(\Delta a_{\ell,n}^2 \Delta t_\ell) \mathbf{1}_{\Delta a_{\ell,n}^2 > 0} - \mathcal{Q}''_n(-\Delta a_{\ell,n}^2 \Delta t_\ell) \mathbf{1}_{\Delta a_{\ell,n}^2 < 0} \right),\end{aligned}$$

where $\Delta a_{\ell-1,n}^1 = a(\bar{X}_\ell(t_n)) - a(\bar{X}_{\ell-1}(t_n))$ and $\Delta a_{\ell-1,n}^2 = a(\bar{X}_\ell(t_n + \Delta t_\ell)) - a(\bar{X}_{\ell-1}(t_n))$.

In the following, we denote

$$(2.6) \quad \Delta a_{\ell,n} = \begin{cases} |\Delta a_{\ell-1,n}^1|, & \text{in } [t_n, t_n + \Delta t_\ell]. \\ |\Delta a_{\ell-1,n}^2|, & \text{in } [t_n + \Delta t_\ell, t_{n+1}]. \end{cases}$$

Remark 2.1. Note that in (2.5), not only are $\mathcal{P}'_n, \mathcal{P}''_n, \mathcal{Q}'_n, \mathcal{Q}''_n$ rdvs, but $\Delta a_{\ell,n}$ is also a random variable because of its dependence on $\bar{X}_{\ell-1}(t_n), \bar{X}_\ell(t_n)$, and $\bar{X}_\ell(t_n + \Delta t_\ell)$. Therefore, to derive some of the following formulas for analyzing our importance sampling algorithm, we need to consider a sigma-algebra, \mathcal{F}_n , such that $\Delta a_{\ell,n}$, conditioned on \mathcal{F}_n , is deterministic, *i.e.*, $\Delta a_{\ell,n}$ is measurable with respect to \mathcal{F}_n . In this way, the only randomness that we consider comes from the Poisson rdvs used for updating the states of $\bar{X}_\ell(t_{n+1})$ and $\bar{X}_{\ell-1}(t_{n+1})$. For this purpose, we consider for a fixed n , \mathcal{F}_n as the sigma algebra

$$(2.7) \quad \mathcal{F}_n := \sigma \left((\Delta a_k)_{k=1, \dots, n} \right), \quad n = 1, \dots, N_\ell.$$

By conditioning on \mathcal{F}_n , using (2.5) recursively, and summing up over the number of time steps of the fine level, N_ℓ , we end up with

$$\begin{aligned}
(2.8) \quad |\Delta \bar{X}_\ell| &= |\bar{X}_\ell(T) - \bar{X}_{\ell-1}(T)| \leq |\nu_1| \sum_{n=1}^{N_\ell} \mathcal{P}_n(\Delta a_{\ell,n} \Delta t_\ell) \\
&\approx |\nu_1| \mathcal{P} \left(\sum_{n=1}^{N_\ell} \Delta a_{\ell,n} \Delta t_\ell \right) \\
&\approx |\nu_1| \mathcal{P}(\Lambda_\ell \Delta t_\ell),
\end{aligned}$$

where \mathcal{P} is some Poisson random variable, $\{\mathcal{P}_n\}_{n=1}^{N_\ell}$ are independent Poisson rdvs, and $\Lambda_\ell = \sum_{n=1}^{N_\ell} \Delta a_{\ell,n}$.

Using (2.8) and taking $|\nu_1| = 1$ for simplicity, we obtain

$$(2.9) \quad \mathbb{P}(\Delta \bar{X}_\ell = k \mid \mathcal{F}_{N_\ell}) \approx e^{-\Lambda_\ell \Delta t_\ell} \frac{(\Lambda_\ell \Delta t_\ell)^k}{k!}, \quad k = 0, 1, \dots,$$

while the near optimal one is given by

$$(2.10) \quad \pi(\Delta \bar{X}_\ell = k \mid \mathcal{F}_{N_\ell}) \propto k \mathbb{P}(\Delta \bar{X}_\ell = k \mid \mathcal{F}_{N_\ell}) = k e^{-\Lambda_\ell \Delta t_\ell} \frac{(\Lambda_\ell \Delta t_\ell)^k}{k!}, \quad k = 1, 2, \dots,$$

which kills the event $\{\Delta \bar{X}_\ell = 0\}$, where most of \mathbb{P} lives, implying a substantial change. In fact, we can observe that before the change of measure, for $\Lambda_\ell \Delta t_\ell \ll 1$, $\mathbb{P}(\Delta \bar{X}_\ell = 0 \mid \mathcal{F}_{N_\ell}) \approx (1 - \Lambda_\ell \Delta t_\ell)$, and after the change of measure, we have $\pi(\Delta \bar{X}_\ell = 0 \mid \mathcal{F}_{N_\ell}) = 0$.

The above discussion indicates that the near optimal measure change creates at least one jump over a single entire trajectory, and sampling from π is the same as sampling from \mathbb{P} but with the events being shifted by -1 and the zero event disappearing. Unfortunately, it is unfeasible to sample from π ; therefore, our goal in the following section is to propose a practical importance sampling algorithm with a sub-optimal change of measure that is close to the optimal measure π .

2.2 On the choice of the new measure and the importance sampling algorithm

In this section, we describe how we choose the new measure to be used for importance sampling. Instead of using $\Delta a_{\ell,n} \Delta t_\ell$ as the rate parameter of the Poisson rdvs used in each time step to update the states of the coupled paths (2.3, 2.4) where $\Delta a_{\ell,n}$ is given by (2.6), we suggest to use $\lambda_{\ell,n} \Delta t_\ell$, with the parameter $\lambda_{\ell,n}$ that will be determined given some constraints that we impose to ensure that our change of measure is i) reducing the kurtosis of the MLMC estimator at the deep levels, ii) reducing, if possible, the variance of the MLMC levels (or even increasing the strong convergence rate if possible), which may improve the complexity of the MLMC estimator.

2.2.1 One dimensional case

We start with the one dimensional case (only one species), where the number of reactions is ($J = 1$) (in this case we denote the state change scalar by ν_1 ; see (1.1)), and we consider $g(x) = x$, $x \in \mathbb{R}$. The simpler choice of g is essentially to make the analysis as simple as possible, but note that the below analysis holds for any Lipschitz function g . We also recall that the change of measure is

performed at each time step by going forward in time, and is only applied when it is needed, *i.e.*, we impose a condition for applying the change of measure given by

$$(2.11) \quad \Delta a_{n,\ell} \neq 0 \quad \& \quad \Delta g_\ell(t_n) = 0, \quad 1 \leq n \leq N_\ell, \quad \ell = 1, \dots, L.$$

Condition (2.11) is motivated by the fact that i) we need to change the measure only in cases where the coupled paths at the n th time step are equal and ii) for cases where the rates of the Poisson rdvs are non zero so we do not have the issue of the likelihood being equal to zero.

In the following, we derive the expression of the likelihood ratio at each time step conditional on \mathcal{F}_n (defined in (2.7)). This helps to determine the optimal choice of the new measure.

We start by writing the conditional likelihood $L_{\ell,n} \mid \mathcal{F}_n$ at level ℓ and for each n th time step we apply the change of measure, which is given by

$$\begin{aligned} L_{\ell,n} \mid \mathcal{F}_n &= \frac{e^{\Delta a_{\ell,n} \Delta t_\ell}}{e^{\lambda_{\ell,n} \Delta t_\ell}} \left(\frac{\Delta a_{\ell,n}}{\lambda_{\ell,n}} \right)^{k_n}, \quad n \in \mathcal{I}_\ell^s \\ &= e^{\Delta t_\ell (\Delta a_{\ell,n} - \lambda_{\ell,n})} \left(\frac{\Delta a_{\ell,n}}{\lambda_{\ell,n}} \right)^{k_n}, \end{aligned}$$

where k_n is the number of jumps that occurs at the n th time step where we apply the change of measure, and \mathcal{I}_ℓ^s is the set including the time steps at level ℓ where we simulate the Poisson rdvs under the new measure.

Thus, across one path, the likelihood factor is given by

$$L_\ell \mid (\mathcal{F}_{N_\ell}, \mathcal{I}_\ell^s = \mathcal{S}) = \prod_{n \in \mathcal{S}} L_{\ell,n} \mid \mathcal{F}_n = e^{\Delta t_\ell \sum_{n \in \mathcal{S}} (\Delta a_{\ell,n} - \lambda_{\ell,n})} \prod_{n \in \mathcal{S}} \left(\frac{\Delta a_{\ell,n}}{\lambda_{\ell,n}} \right)^{k_n}.$$

Furthermore, if we impose that $\lambda_{\ell,n} = c_\ell \Delta a_{\ell,n}$ then we obtain

$$(2.12) \quad L_\ell \mid (\mathcal{F}_{N_\ell}, \mathcal{I}_\ell^s = \mathcal{S}) = \left(e^{(c_\ell - 1) \Delta t_\ell \sum_{n \in \mathcal{S}} \Delta a_{\ell,n}} \right) \left(c_\ell^{-\sum_{n \in \mathcal{S}} k_n} \right).$$

We note that imposing $\lambda_{\ell,n} = c_\ell \Delta a_{\ell,n}$ can be motivated by the fact that we want to keep the same physical structure of the rate of the Poisson process driving the state changes, *i.e.*, depending on $\Delta a_{\ell,n}$. However, we try to introduce a scaled constant c_ℓ that depends on Δt_ℓ so that we reduce the probability of having $\Delta g_\ell(T) = 0$, under the new measure.

In the following, we try to determine the optimal choice of c_ℓ . Due to Section 2.1 and the conditioning done at each n th time step with respect to \mathcal{F}_n as defined in (2.7), we can write

$$(2.13) \quad \begin{aligned} |g_\ell(T) - g_{\ell-1}(T)| &= |\bar{X}_\ell(T) - \bar{X}_{\ell-1}(T)| \\ &\leq |\nu_1| \left(\underbrace{\sum_{n \in \mathcal{I}_\ell^s} \mathcal{P}_n(c_\ell \Delta a_{\ell,n} \Delta t_\ell)}_{\text{steps simulated with the new measure}} + \underbrace{\sum_{n=1, n \notin \mathcal{I}_\ell^s}^{N_\ell} \mathcal{R}_n(\Delta a_{\ell,n} \Delta t_\ell)}_{\text{steps simulated with the true (old) measure}} \right) \\ &\approx |\nu_1| \left(\underbrace{\bar{\mathcal{P}} \left(\sum_{n \in \mathcal{I}_\ell^s} c_\ell \Delta a_{\ell,n} \Delta t_\ell \right)}_{\text{steps simulated with the new measure}} + \underbrace{\bar{\mathcal{R}} \left(\sum_{n=1, n \notin \mathcal{I}_\ell^s}^{N_\ell} \Delta a_{\ell,n} \Delta t_\ell \right)}_{\text{steps simulated with the true (old) measure}} \right), \end{aligned}$$

where $\{\mathcal{P}_n\}_{n \in \mathcal{I}_\ell^s}$ and $\{\mathcal{R}_n\}_{n=1, n \notin \mathcal{I}_\ell^s}^{N_\ell}$ are independent Poisson rdvs, and also $\bar{\mathcal{P}}$ and $\bar{\mathcal{R}}$ are independent Poisson rdvs.

Observe that

$$(2.14) \quad \text{Prob} \left(\bar{\mathcal{R}} \left(\sum_{\substack{n=1 \\ n \notin \mathcal{I}_\ell^s}}^{N_\ell} \Delta a_{\ell, n} \Delta t_\ell \right) = 0; (\mathcal{F}_{N_\ell}, \mathcal{I}_\ell^s = \mathcal{S}) \right) = e^{-\left(\sum_{n=1, n \notin \mathcal{I}_\ell^s}^{N_\ell} \Delta a_{\ell, n} \Delta t_\ell \right)} \approx 1 - \left(\sum_{n=1, n \notin \mathcal{I}_\ell^s}^{N_\ell} \Delta a_{\ell, n} \Delta t_\ell \right) \xrightarrow{\Delta t_\ell \rightarrow 0} 1,$$

and

$$(2.15) \quad \text{Prob} \left(\bar{\mathcal{P}} \left(c_\ell \Delta t_\ell \sum_{n \in \mathcal{I}_\ell^s} \Delta a_{\ell, n} \right) = 0; (\mathcal{F}_{N_\ell}, \mathcal{I}_\ell^s = \mathcal{S}) \right) = e^{-\left(c_\ell \Delta t_\ell \sum_{n \in \mathcal{I}_\ell^s} \Delta a_{\ell, n} \right)}.$$

Therefore, using the conditional independence and due to (2.13), (2.14), and (2.15)

$$(2.16) \quad \begin{aligned} & \text{Prob} (|\Delta \bar{X}_\ell(T)| = |\bar{X}_\ell(T) - \bar{X}_{\ell-1}(T)| = 0; (\mathcal{F}_{N_\ell}, \mathcal{I}_\ell^s = \mathcal{S})) \\ & \approx \text{Prob} \left(\bar{\mathcal{P}} \left(\sum_{n \in \mathcal{I}_\ell^s} \Delta a_{\ell, n} \Delta t_\ell \right) = 0; (\mathcal{F}_{N_\ell}, \mathcal{I}_\ell^s = \mathcal{S}) \right) \times \underbrace{\text{Prob} \left(\bar{\mathcal{R}} \left(\sum_{n \notin \mathcal{I}_\ell^s} \Delta a_{\ell, n} \Delta t_\ell \right) = 0; (\mathcal{F}_{N_\ell}, \mathcal{I}_\ell^s = \mathcal{S}) \right)}_{\xrightarrow{\Delta t_\ell \rightarrow 0} 1} \\ & \approx \text{Prob} \left(\bar{\mathcal{P}} \left(c_\ell \Delta t_\ell \sum_{n \in \mathcal{I}_\ell^s} \Delta a_{\ell, n} \right) = 0; (\mathcal{F}_{N_\ell}, \mathcal{I}_\ell^s = \mathcal{S}) \right) \\ & = e^{-\left(c_\ell \Delta t_\ell \sum_{n \in \mathcal{I}_\ell^s} \Delta a_{\ell, n} \right)}. \end{aligned}$$

Then the first criterion for choosing c_ℓ is to make the right-hand side of (2.16) as small as possible compared to the case of using the old measure, and this can be achieved by choosing c_ℓ

$$(2.17) \quad c_\ell = \Delta t_\ell^{-\delta},$$

where $\delta > 0$ is the scale parameter to be determined. Note that the case $\delta = 0$ is similar to the case of using the old measure in all time steps. Furthermore, looking just at (2.16) suggests making δ as large as possible.

Remark 2.2. Observe that by choosing $\delta \in (0, 1)$ or $\delta \in [1, +\infty)$, we can have different behaviors for (2.16). In fact, if $\delta \in (0, 1)$, $\text{Prob} (|\Delta \bar{X}_\ell(T)| = 0; (\mathcal{F}_{N_\ell}, \mathcal{I}_\ell^s = \mathcal{S}))$ still becomes very close to 1 for small values of Δt_ℓ , but compared to the initial situation (without importance sampling), we decrease the rate of convergence with respect to Δt_ℓ (compare Figure 3.3, for the case without importance sampling, and Figure 3.4 for the case with importance sampling with $\delta = \frac{3}{4}$). On the other hand, by selecting $\delta \in [1, +\infty)$, we kill the zero event and $\text{Prob} (|\Delta \bar{X}_\ell(T)| = 0; (\mathcal{F}_{N_\ell}, \mathcal{I}_\ell^s = \mathcal{S}))$ becomes very close to 0 for small values of Δt_ℓ .

The next task is to check if we have an upper bound on the choice of δ , and this can be obtained by looking at the conditional kurtosis κ_ℓ of $|g_\ell - g_{\ell-1}|(T)L_\ell$ conditioned on \mathcal{F}_{N_ℓ} and $\mathcal{I}_\ell^s = \mathcal{S}$.

First, observe that, for small Δt_ℓ , and conditioned on \mathcal{F}_{N_ℓ} and $\mathcal{I}_\ell^s = \mathcal{S}$, we have

$$(2.18) \quad |g_\ell - g_{\ell-1}|(T) \approx |\nu_1| \sum_{n \in \mathcal{S}} k_n.$$

Then, if we denote by $L_\ell | (\mathcal{F}_{N_\ell}, \mathcal{I}_\ell^s = \mathcal{S}) (\alpha)$ the conditioned likelihood evaluated at $\sum_{n \in \mathcal{S}} k_n = \alpha$, we can approximate $\mathbb{E} [|g_\ell - g_{\ell-1}|^p(T) L_\ell^p; (\mathcal{F}_{N_\ell}, \mathcal{I}_\ell^s = \mathcal{S})]$ as

$$(2.19) \quad \begin{aligned} & \mathbb{E} [|g_\ell - g_{\ell-1}|^p(T) L_\ell^p; (\mathcal{F}_{N_\ell}, \mathcal{I}_\ell^s = \mathcal{S})] \\ & \approx |\nu_1|^p (L_\ell | (\mathcal{F}_{N_\ell}, \mathcal{I}_\ell^s = \mathcal{S}))^p (1) \text{Prob}(|g_\ell - g_{\ell-1}|(T) = |\nu_1|; (\mathcal{F}_{N_\ell}, \mathcal{I}_\ell^s = \mathcal{S})) \\ & + (2|\nu_1|)^p (L_\ell | (\mathcal{F}_{N_\ell}, \mathcal{I}_\ell^s = \mathcal{S}))^p (2) \text{Prob}(|g_\ell - g_{\ell-1}|(T) = 2|\nu_1|; (\mathcal{F}_{N_\ell}, \mathcal{I}_\ell^s = \mathcal{S})) \\ & + \dots \end{aligned}$$

Then using (2.12), (2.18) and (2.19), we have

$$(2.20) \quad \begin{aligned} & \mathbb{E} [|g_\ell - g_{\ell-1}|^p(T) L_\ell^p; (\mathcal{F}_{N_\ell}, \mathcal{I}_\ell^s = \mathcal{S})] \\ & \approx |\nu_1|^p e^{p(\Delta t_\ell^{1-\delta} - \Delta t_\ell) \sum_{n \in \mathcal{S}} \Delta a_{\ell,n}} \left(\Delta t_\ell^{p\delta} \right) e^{-(\Delta t_\ell^{1-\delta} \sum_{n \in \mathcal{S}} \Delta a_{\ell,n})} \left(\Delta t_\ell^{1-\delta} \sum_{n \in \mathcal{S}} \Delta a_{\ell,n} \right) \\ & + (2|\nu_1|)^p e^{p(\Delta t_\ell^{1-\delta} - \Delta t_\ell) \sum_{n \in \mathcal{S}} \Delta a_{\ell,n}} \left(\Delta t_\ell^{2p\delta} \right) \frac{1}{2} e^{-(\Delta t_\ell^{1-\delta} \sum_{n \in \mathcal{S}} \Delta a_{\ell,n})} \left(\Delta t_\ell^{1-\delta} \sum_{n \in \mathcal{S}} \Delta a_{\ell,n} \right)^2 \\ & + \dots \end{aligned}$$

Remark 2.3. The ratio of the second term to the first term on the right-hand side of (2.20) is equal to $2^{p-1} \Delta t_\ell^{1+(p-1)\delta} \sum_{n \in \mathcal{S}} \Delta a_{\ell,n}$, which suggests that for $p \geq 1$, we have $1 + (p-1)\delta > 0$ and then the first term is significantly dominating the remaining terms of (2.20), as $\Delta t_\ell \rightarrow 0$.

Therefore, due to remark 2.3, the conditioned kurtosis κ_ℓ can be approximated by

$$(2.21) \quad \begin{aligned} \kappa_\ell & \approx \frac{\mathbb{E} [|g_\ell - g_{\ell-1}|^4(T) L_\ell^4; (\mathcal{F}_{N_\ell}, \mathcal{I}_\ell^s = \mathcal{S})]}{\mathbb{E} [|g_\ell - g_{\ell-1}|^2(T) L_\ell^2; (\mathcal{F}_{N_\ell}, \mathcal{I}_\ell^s = \mathcal{S})]^2} \\ & \approx \frac{1}{\text{Prob}(|g_\ell - g_{\ell-1}|(T) = |\nu_1|; (\mathcal{F}_{N_\ell}, \mathcal{I}_\ell^s = \mathcal{S}))} \\ & = \left(\Delta t_\ell^{\delta-1} \right) \left(\sum_{n \in \mathcal{S}} \Delta a_{\ell,n} \right)^{-1} e^{(\Delta t_\ell^{1-\delta} \sum_{n \in \mathcal{S}} \Delta a_{\ell,n})}. \end{aligned}$$

The approximation formula (2.21) shows clearly the effect seen for the limiting case $\delta = 0$ where we do not apply the importance sampling algorithm and thus, the kurtosis κ_ℓ increases with rate Δt_ℓ^{-1} . The optimal range for δ should be in $(0, 1)$ since any $\delta \geq 1$ may excite the exponential term with negative effects on the kurtosis. In conclusion, Formula (2.21) suggests to take δ to be as large as possible, in $(0, 1)$. Compared to the case without importance sampling, we see clearly that we reduce the kurtosis by a factor of $\Delta t_\ell^{-\delta}$, given that the exponential term converges to 1 for small values of Δt_ℓ . These observations are confirmed by our numerical experiments in Section 3.

Remark 2.4. Note that the minimization problem of (2.21) has a clear optimal solution

$$(2.22) \quad \delta^* = 1 + \frac{\log\left(\sum_{n \in \mathcal{S}} \Delta a_{\ell, n}\right)}{\log(\Delta t_{\ell})}.$$

Although (2.22) is difficult to work with in practice because a priori estimate of $\sum_{n \in \mathcal{S}} \Delta a_{\ell, n}$ is needed, it gives us some insights about the choice of a sub-optimal δ . In fact, since $\sum_{n \in \mathcal{S}} \Delta a_{\ell, n} = \mathcal{O}(1)$, we have $\delta^* \xrightarrow{\Delta t_{\ell} \rightarrow 0} 1$. This observation suggests that we may start with a given δ_0 at the coarsest level of MLMC and then build a hierarchy of δ_{ℓ} such that $\delta_{\ell} \xrightarrow{\ell \rightarrow L} 1$. In this work, we opt to use a uniform $\delta \in (0, 1)$ for our numerical experiments; studying the use of hierarchical δ_{ℓ} is left for a future work.

Now, let us fix $\delta \in (0, 1)$. Regarding the strong convergence rate, we can easily show that $\text{Var}(|g_{\ell} - g_{\ell-1}|(T)L_{\ell}; (\mathcal{F}_{N_{\ell}}, \mathcal{I}_{\ell}^s = \mathcal{S})) = \mathcal{O}\left(\Delta t_{\ell}^{1+\delta}\right)$, as will be confirmed by our numerical experiments in Section 3. Using (2.20) and Remark 2.3, we have

$$\begin{aligned} & \text{Var}(|g_{\ell} - g_{\ell-1}|(T)L_{\ell}; (\mathcal{F}_{N_{\ell}}, \mathcal{I}_{\ell}^s = \mathcal{S})) \\ &= \mathbb{E} \left[|g_{\ell} - g_{\ell-1}|^2 (T)L_{\ell}^2; (\mathcal{F}_{N_{\ell}}, \mathcal{I}_{\ell}^s = \mathcal{S}) \right] - (\mathbb{E}[|g_{\ell} - g_{\ell-1}|(T)L_{\ell}; (\mathcal{F}_{N_{\ell}}, \mathcal{I}_{\ell}^s = \mathcal{S})])^2 \\ &\propto \Delta t_{\ell}^{1+\delta} \underbrace{\left(e^{2(\Delta t_{\ell}^{1-\delta} - \Delta t_{\ell}) \sum_{n \in \mathcal{S}} \Delta a_{\ell, n}} \right)}_{\xrightarrow{\Delta t_{\ell} \rightarrow 0} 1} \underbrace{e^{-(\Delta t_{\ell}^{1-\delta} \sum_{n \in \mathcal{S}} \Delta a_{\ell, n})}}_{\xrightarrow{\Delta t_{\ell} \rightarrow 0} 1} \underbrace{\left(\sum_{n \in \mathcal{S}} \Delta a_{\ell, n} \right)}_{\mathcal{O}(1)} \\ &\quad \times \underbrace{\left(1 - e^{-(\Delta t_{\ell}^{1-\delta} \sum_{n \in \mathcal{S}} \Delta a_{\ell, n})} \left(\Delta t_{\ell}^{1-\delta} \sum_{n \in \mathcal{S}} \Delta a_{\ell, n} \right) \right)}_{\xrightarrow{\Delta t_{\ell} \rightarrow 0} 1} \\ &= \mathcal{O}\left(\Delta t_{\ell}^{1+\delta}\right). \end{aligned}$$

Our above analysis, confirmed by the conducted numerical experiments in Section 3, demonstrates that our importance sampling algorithm improves the strong convergence rate from $\beta = 1$ (see Figure 3.2 for Example 3.1) for the case without importance sampling, to $\beta = 1 + \delta$ with $\delta > 0$ (see Figures 3.5, 3.6 and 3.7 for Example 3.1) for the case with importance sampling. Due to Theorem 1.1 for the complexity of MLMC method, and given that $\gamma = 1$ (work rate) for both cases, with and without importance sampling, we improve the complexity from $\mathcal{O}(TOL^{-2} \log(TOL)^2)$ for the case without importance sampling (since $\beta = \gamma$) to $\mathcal{O}(TOL^{-2})$ for the case with importance sampling (since $\beta > \gamma$), where TOL is a pre-selected tolerance.

2.2.2 Generalization of our method to multi-channels and high dimensional states

Extending our method to a higher dimension in the number of reaction channels, J , and in the state vector \mathbf{X} is straightforward with slight modifications. We first define the set \mathcal{J}_1 as

$$\mathcal{J}_1 = \{1 \leq j \leq J; \quad g(\mathbf{X} + \boldsymbol{\nu}_j) \neq g(\mathbf{X})\}.$$

In the multi-channel case, we are only interested in changing the measure for reactions whose stoichiometric vector, $\boldsymbol{\nu}_j$, changes the state of the QoI, *i.e.*, for reactions with index $j \in \mathcal{J}_1$. In Algorithm 2.1, we summarize our methodology for simulating two coupled explicit TL paths with importance sampling.

Algorithm 2.1 Simulates two coupled explicit TL paths with importance sampling.

```

1: Fix  $\Delta t_\ell > 0$  and set  $\Delta t_{\ell-1} = 2 \times \Delta t_\ell$ .
2: Set  $\mathbf{Z}_\ell(0) = \mathbf{Z}_{\ell-1}(0) = \mathbf{x}_0$ ,  $t_\ell = t_{\ell-1} = 0$ ,  $n=0$ .
3: Set  $c_\ell = \Delta t_\ell^{-\delta}$ ,  $\delta \in (0, 1)$ 
4: while  $t_\ell < T$  do
5:    $n = n + 1$ 
6:   for  $j=1$  to  $J$  do
7:     if then  $(a_j(\mathbf{Z}_\ell(t_\ell)) \neq a_j(\mathbf{Z}_{\ell-1}(t_{\ell-1})) \ \& \ g(\mathbf{Z}_\ell(t_\ell)) = g(\mathbf{Z}_{\ell-1}(t_\ell)) \ \& \ j \in \mathcal{J}_1)$ 
8:        $A_{3(j-1)+1} = a_j(\mathbf{Z}_\ell(t_\ell)) \wedge a_j(\mathbf{Z}_{\ell-1}(\Delta t_{\ell-1}))$ 
9:        $A_{3(j-1)+2} = c_\ell (a_j(\mathbf{Z}_\ell(t_\ell)) - A_{3(j-1)+1})$ 
10:       $A_{3(j-1)+3} = c_\ell (a_j(\mathbf{Z}_{\ell-1}(t_{\ell-1})) - A_{3(j-1)+1})$ 
11:     else
12:        $A_{3(j-1)+1} = a_j(\mathbf{Z}_\ell(t_\ell)) \wedge a_j(\mathbf{Z}_{\ell-1}(t_{\ell-1}))$ 
13:        $A_{3(j-1)+2} = a_j(\mathbf{Z}_\ell(t_\ell)) - A_{3(j-1)+1}$ 
14:        $A_{3(j-1)+3} = a_j(\mathbf{Z}_{\ell-1}(t_{\ell-1})) - A_{3(j-1)+1}$ 
15:        $\Lambda_{3(j-1)+1} = \text{Poisson}(A_{3(j-1)+1} \Delta t_\ell)$ 
16:        $\Lambda_{3(j-1)+2} = \text{Poisson}(A_{3(j-1)+2} \Delta t_\ell)$ 
17:        $\Lambda_{3(j-1)+3} = \text{Poisson}(A_{3(j-1)+3} \Delta t_\ell)$ 
18:     State updating
19:     i) Set  $\mathbf{\Gamma}_\ell = \boldsymbol{\nu} \otimes [1 \ 1 \ 0]$  and  $\mathbf{\Gamma}_{\ell-1} = \boldsymbol{\nu} \otimes [1 \ 0 \ 1]$  ( $A \otimes B$  refers to the Kronecker product of the matrices  $A$  and  $B$ ).
20:     ii) Update  $\mathbf{Z}_\ell(t_\ell + \Delta t_\ell) = \mathbf{Z}_\ell(t_\ell) + \Delta t_\ell \mathbf{\Gamma}_\ell \Lambda$ 
21:     iii) Update  $\mathbf{Z}_{\ell-1}(t_\ell + \Delta t_\ell) = \mathbf{Z}_{\ell-1}(t_\ell) + \Delta t_\ell \mathbf{\Gamma}_{\ell-1} \Lambda$ 
22:     if  $(n \bmod 2) = 0$  then  $t_{\ell-1} = t_{\ell-1} + \Delta t_{\ell-1}$ 
23:      $t_\ell = t_\ell + \Delta t_\ell$ 

```

To extend the analysis carried out in Section 2.1 to the higher dimensional case, we consider a number of reaction $J > 1$, $\mathbf{X} \in \mathbb{R}^d$, $d \geq 1$ and for $g : \mathbb{R}^d \rightarrow \mathbb{R}$, for example $g(\mathbf{X}) = X^{(i)}$, *i.e.*, the projection on the i th coordinate of the state vector X . The simpler choice of g is essentially to make the analysis as simple as possible but the below analysis holds for any Lipschitz function g . Hereafter, we denote by $\{\nu_{j,i}\}_{j=1}^J$ the coordinates in the stoichiometric vectors, $\{\boldsymbol{\nu}_j\}_{j=1}^J$, corresponding to the state change of the i th species.

For the high dimensional case, we consider for a fixed n , \mathcal{F}_n as the sigma algebra

$$(2.23) \quad \mathcal{F}_n := \sigma \left(\left(\Delta a_k^j \right)_{j=1, \dots, J; k=1, \dots, n} \right), \quad n = 1, \dots, N_\ell.$$

From Algorithm 2.1, we consider the conditioned likelihood factor for each reaction channel $j \in \mathcal{J}_1$,

having a similar expression to (2.12), and given by

$$L_\ell^j \mid (\mathcal{F}_{N_\ell}, \mathcal{I}_{\ell,j}^s = S_j) = \left(e^{(c_\ell-1)\Delta t_\ell \sum_{n \in S_j} \Delta a_{\ell,n}^j} \right) \left(c_\ell^{-\sum_{n \in S_j} k_n^j} \right), \quad j \in \mathcal{J}_1,$$

where k_n^j is the number of jumps associated with the j th reaction channel that occurs at the n th time step where we apply the change of measure, and $\mathcal{I}_{\ell,j}^s$ is the set including the time steps at level ℓ where we simulate the Poisson rdvs under the new measure for the j th reaction channel.

Due to the independence assumption between all reaction channels, the total conditioned likelihood factor is given by

$$L_\ell \mid (\mathcal{F}_{N_\ell}, (\mathcal{I}_{\ell,j}^s = S_j)_{j \in \mathcal{J}}) = \prod_{j \in \mathcal{J}_1} L_\ell^j \mid (\mathcal{F}_{N_\ell}, \mathcal{I}_{\ell,j}^s = S_j) = \left(e^{(c_\ell-1)\Delta t_\ell \sum_{j \in \mathcal{J}_1} \sum_{n \in S_j} \Delta a_{\ell,n}^j} \right) \left(c_\ell^{-\sum_{j \in \mathcal{J}_1} \sum_{n \in S_j} k_n^j} \right).$$

Conditioning on \mathcal{F}_{N_ℓ} defined in (2.23), we can also extend (2.13) to

$$\begin{aligned} |g_\ell(T) - g_{\ell-1}(T)| &= \left| \overline{X}_\ell^{(i)}(T) - \overline{X}_{\ell-1}^{(i)}(T) \right| \\ &\leq \sum_{j \notin \mathcal{J}_1} |\nu_{j,i}| \left(\underbrace{\sum_{n=1}^{N_\ell} \mathcal{R}_{n,j} \left(\Delta a_{\ell,n}^j \Delta t_\ell \right)}_{\text{steps simulated with the true (old) measure}} \right) \\ &\quad + \sum_{j \in \mathcal{J}_1} |\nu_{j,i}| \left(\underbrace{\sum_{n \in \mathcal{I}_{\ell,j}^s} \mathcal{P}_{n,j} \left(c_\ell \Delta a_{\ell,n}^j \Delta t_\ell \right)}_{\text{steps simulated with the new measure}} + \underbrace{\sum_{n=1, n \notin \mathcal{I}_{\ell,j}^s}^{N_\ell} \mathcal{R}_{n,j} \left(\Delta a_{\ell,n}^j \Delta t_\ell \right)}_{\text{steps simulated with the true (old) measure}} \right) \\ (2.24) \quad &\approx \sum_{j \notin \mathcal{J}_1} |\nu_{j,i}| \left(\underbrace{\overline{\mathcal{R}}_j \left(\sum_{n=1}^{N_\ell} \Delta a_{\ell,n}^j \Delta t_\ell \right)}_{\text{steps simulated with the true (old) measure}} \right) \\ &\quad + \sum_{j \in \mathcal{J}_1} |\nu_{j,i}| \left(\underbrace{\overline{\mathcal{P}}_j \left(\sum_{n \in \mathcal{I}_{\ell,j}^s} c_\ell \Delta a_{\ell,n}^j \Delta t_\ell \right)}_{\text{steps simulated with the new measure}} + \underbrace{\overline{\mathcal{R}}_j \left(\sum_{n=1, n \notin \mathcal{I}_{\ell,j}^s}^{N_\ell} \Delta a_{\ell,n}^j \Delta t_\ell \right)}_{\text{steps simulated with the true (old) measure}} \right), \end{aligned}$$

where $\{\mathcal{P}_{n,j}\}_{n \in \mathcal{I}_{\ell,j}^s, j \in \mathcal{J}_1}$, $\{\mathcal{R}_{n,j}\}_{n \notin \mathcal{I}_{\ell,j}^s, j \in \mathcal{J}_1}$, and $\{\mathcal{R}_{n,j}\}_{1 \leq n \leq N_\ell, j \notin \mathcal{J}_1}$ are independent Poisson rdvs, and also $\{\overline{\mathcal{P}}_j\}_{j \in \mathcal{J}_1}$ and $\{\overline{\mathcal{R}}_j\}_{j \notin \mathcal{J}_1}$ are independent Poisson rdvs.

Using the conditional independence, and due to (2.24), (2.14), and (2.15), we have

$$\begin{aligned}
& \text{Prob} \left(|\Delta g_\ell(T)| = |g(\bar{\mathbf{X}}_\ell(T)) - g(\bar{\mathbf{X}}_{\ell-1}(T))| = 0; \left(\mathcal{F}_{N_\ell}, (\mathcal{I}_{\ell,j}^s = S_j)_{j \in \mathcal{J}} \right) \right) \\
& \approx \prod_{j \in \mathcal{J}_1} \text{Prob} \left(\bar{\mathcal{P}}_j \left(\sum_{n \in \mathcal{I}_{\ell,j}^s} \Delta a_{\ell,n}^j \Delta t_\ell \right) = 0; (\mathcal{F}_{N_\ell}, \mathcal{I}_{\ell,j}^s = S_j) \right) \\
& \times \underbrace{\prod_{j \in \mathcal{J}_1} \text{Prob} \left(\bar{\mathcal{R}}_j \left(\sum_{n \notin \mathcal{I}_{\ell,j}^s} \Delta a_{\ell,n}^j \Delta t_\ell \right) = 0; (\mathcal{F}_{N_\ell}, \mathcal{I}_{\ell,j}^s = S_j) \right)}_{\xrightarrow{\Delta t_\ell \rightarrow 0} 1} \times \underbrace{\prod_{j \notin \mathcal{J}_1} \text{Prob} \left(\bar{\mathcal{R}}_j \left(\sum_{n=1}^{N_\ell} \Delta a_{\ell,n}^j \Delta t_\ell \right) = 0; \mathcal{F}_{N_\ell} \right)}_{\xrightarrow{\Delta t_\ell \rightarrow 0} 1} \\
& \approx \prod_{j \in \mathcal{J}_1} \text{Prob} \left(\bar{\mathcal{P}}_j \left(\sum_{n \in \mathcal{I}_{\ell,j}^s} \Delta a_{\ell,n}^j \Delta t_\ell \right) = 0; (\mathcal{F}_{N_\ell}, \mathcal{I}_{\ell,j}^s = S_j) \right) \\
(2.25) \quad & = e^{-\sum_{j \in \mathcal{J}_1} (c_\ell \Delta t_\ell \sum_{n \in \mathcal{S}_j} \Delta a_{\ell,n}^j)}.
\end{aligned}$$

Similarly to Section 2.2.1 and from (2.25), we conclude that c_ℓ as given by (2.17), with $\delta > 0$.

Remark 2.5. Remark 2.2 holds for the high dimensional case. For instance, compare Figures 3.9 and 3.14, for the case without importance sampling, and Figures 3.10 and 3.15 for the case using importance sampling with $\delta = \frac{3}{4}$.

Similarly to the one dimensional case, to get an upper bound for δ , we focus on the conditional kurtosis κ_ℓ . Furthermore, similarly to observation (2.18) (for the one dimensional case), observe that for small Δt_ℓ , and conditioned on \mathcal{F}_{N_ℓ} and $(\mathcal{I}_{\ell,j}^s = S_j)_{j \in \mathcal{J}}$

$$(2.26) \quad |g_\ell - g_{\ell-1}|(T) \approx \left| \sum_{j \in \mathcal{J}_1} \nu_{j,i} \sum_{n \in \mathcal{S}_j} k_n^j \right| = \left| \sum_{j \in \mathcal{J}_1} \nu_{j,i} K_j \right|,$$

where the random variable $K_j = \sum_{n \in \mathcal{S}_j} k_n^j$.

We remind that the conditioned likelihood is given by

$$L_\ell \mid \left(\mathcal{F}_{N_\ell}, (\mathcal{I}_{\ell,j}^s = S_j)_{j \in \mathcal{J}} \right) = \prod_{j \in \mathcal{J}_1} L_\ell^j \mid \left(\mathcal{F}_{N_\ell}, \mathcal{I}_{\ell,j}^s = S_j \right) = \left(e^{(\Delta t_\ell^{1-\delta} - \Delta t_\ell) \sum_{j \in \mathcal{J}_1} \sum_{n \in \mathcal{S}_j} \Delta a_{\ell,n}^j} \right) \left(\Delta t_\ell^\delta \sum_{j \in \mathcal{J}_1} \sum_{n \in \mathcal{S}_j} k_n^j \right).$$

Then, as outlined in Section 2.2.1, the dominant term in $\mathbb{E} \left[|g_\ell - g_{\ell-1}|^p(T) L_\ell^p; \left(\mathcal{F}_{N_\ell}, (\mathcal{I}_{\ell,j}^s = S_j)_{j \in \mathcal{J}} \right) \right]$ will be the sum of terms corresponding to only one jump occurring under the new measure and due to the firing of only one reaction channel $j \in \mathcal{J}_1$, *i.e.*, $\sum_{j \in \mathcal{J}_1} K_j = 1$. Consequently, if we denote

by $L_\ell \mid (\mathcal{F}_{N_\ell}, \mathcal{I}_{\ell,j}^s = S_j) (\alpha_j)$ the conditioned likelihood evaluated at $K_j = \alpha_j$, we have

$$\begin{aligned}
& \mathbb{E} \left[|g_\ell - g_{\ell-1}|^p (T) L_\ell^p; \left(\mathcal{F}_{N_\ell}, (\mathcal{I}_{\ell,j}^s = S_j)_{j \in \mathcal{J}} \right) \right] \\
& \approx \sum_{j \in \mathcal{J}_1} |\nu_{j,i}|^p (L_\ell (\mathcal{F}_{N_\ell}, \mathcal{I}_{\ell,j}^s = S_j))^p (1) \text{Prob} (|g_\ell - g_{\ell-1}| (T) = |\nu_{j,i}|; (\mathcal{F}_{N_\ell}, \mathcal{I}_{\ell,j}^s = S_j)) \\
& \approx \sum_{j \in \mathcal{J}_1} |\nu_{j,i}|^p \left(e^{p(\Delta t_\ell^{1-\delta} - \Delta t_\ell) \sum_{j \in \mathcal{J}_1} \sum_{n \in \mathcal{S}_j} \Delta a_{\ell,n}^j} \right) (\Delta t_\ell^{p\delta}) e^{-(\Delta t_\ell^{1-\delta} \sum_{j \in \mathcal{J}_1} \sum_{n \in \mathcal{S}_j} \Delta a_{\ell,n}^j)} \left(\Delta t_\ell^{1-\delta} \sum_{n \in \mathcal{S}_j} \Delta a_{\ell,n}^j \right) \\
(2.27) \quad & = \left(\Delta t_\ell^{\delta(p-1)+1} \right) \left(e^{p(\Delta t_\ell^{1-\delta} - \Delta t_\ell) \sum_{j \in \mathcal{J}_1} \sum_{n \in \mathcal{S}_j} \Delta a_{\ell,n}^j} \right) e^{-(\Delta t_\ell^{1-\delta} \sum_{j \in \mathcal{J}_1} \sum_{n \in \mathcal{S}_j} \Delta a_{\ell,n}^j)} \left(\sum_{j \in \mathcal{J}_1} |\nu_{j,i}|^p \sum_{n \in \mathcal{S}_j} \Delta a_{\ell,n}^j \right).
\end{aligned}$$

Therefore, similarly to (2.21) for the one dimensional case, and due to (2.27), the conditioned kurtosis κ_ℓ for the high dimensional case can be approximated as

$$(2.28) \quad \kappa_\ell \approx \left(\Delta t_\ell^{\delta-1} \right) e^{(\Delta t_\ell^{1-\delta} \sum_{j \in \mathcal{J}_1} \sum_{n \in \mathcal{S}_j} \Delta a_{\ell,n}^j)} \frac{\sum_{j \in \mathcal{J}_1} |\nu_{j,i}|^4 \sum_{n \in \mathcal{S}_j} \Delta a_{\ell,n}^j}{\left(\sum_{j \in \mathcal{J}_1} |\nu_{j,i}|^2 \sum_{n \in \mathcal{S}_j} \Delta a_{\ell,n}^j \right)^2}.$$

The approximate formula (2.28) shows clearly the effect seen for the limiting case $\delta = 0$ where we do not apply the importance sampling algorithm, and thus the kurtosis κ_ℓ increases with rate Δt_ℓ^{-1} . The optimal range for δ should be in $(0, 1)$, since any $\delta \geq 1$ may excite the exponential term with negative effects on the kurtosis. In conclusion, Formula (2.28) suggests to make δ to be as large as possible, in $(0, 1)$. Compared to the case without importance sampling, we see clearly that we reduce the kurtosis by a factor of $\Delta t_\ell^{-\delta}$, given that the exponential term converges to 1 as $\Delta t_\ell \rightarrow 0$. These observations are confirmed by our numerical experiments in Section 3.

Now, let us fix $\delta \in (0, 1)$. Regarding the strong convergence rate, we can easily show that $\text{Var} \left[|g_\ell - g_{\ell-1}| (T) L_\ell; \left(\mathcal{F}_{N_\ell}, (\mathcal{I}_{\ell,j}^s = S_j)_{j \in \mathcal{J}} \right) \right] = \mathcal{O} \left(\Delta t_\ell^{1+\delta} \right)$, as will be confirmed by our numerical experiments in Section 3. Using (2.27), we have

$$\begin{aligned}
& \text{Var} \left[|g_\ell - g_{\ell-1}| (T) L_\ell; \left(\mathcal{F}_{N_\ell}, (\mathcal{I}_{\ell,j}^s = S_j)_{j \in \mathcal{J}} \right) \right] \\
& = \mathbb{E} \left[|g_\ell - g_{\ell-1}|^2 (T) L_\ell^2; \left(\mathcal{F}_{N_\ell}, (\mathcal{I}_{\ell,j}^s = S_j)_{j \in \mathcal{J}} \right) \right] - \left(\mathbb{E} \left[|g_\ell - g_{\ell-1}| (T) L_\ell; \left(\mathcal{F}_{N_\ell}, (\mathcal{I}_{\ell,j}^s = S_j)_{j \in \mathcal{J}} \right) \right] \right)^2 \\
& \propto \Delta t_\ell^{1+\delta} \underbrace{\left(e^{2(\Delta t_\ell^{1-\delta} - \Delta t_\ell) \sum_{j \in \mathcal{J}_1} \sum_{n \in \mathcal{S}_j} \Delta a_{\ell,n}^j} \right)}_{\xrightarrow[\Delta t_\ell \rightarrow 0]{1}} \underbrace{e^{-(\Delta t_\ell^{1-\delta} \sum_{j \in \mathcal{J}_1} \sum_{n \in \mathcal{S}_j} \Delta a_{\ell,n}^j)}}_{\xrightarrow[\Delta t_\ell \rightarrow 0]{1}} \\
& \times \left(\underbrace{\left(\sum_{j \in \mathcal{J}_1} |\nu_{j,i}|^2 \sum_{n \in \mathcal{S}_j} \Delta a_{\ell,n}^j \right)}_{\mathcal{O}(1)} - \underbrace{e^{-\Delta t_\ell^{1-\delta} (\sum_{j \in \mathcal{J}_1} \sum_{n \in \mathcal{S}_j} \Delta a_{\ell,n}^j)} \Delta t_\ell^{1-\delta} \left(\sum_{j \in \mathcal{J}_1} |\nu_{j,i}| \sum_{n \in \mathcal{S}_j} \Delta a_{\ell,n}^j \right)^2}_{\xrightarrow[\Delta t_\ell \rightarrow 0]{0}} \right) \\
& = \mathcal{O} \left(\Delta t_\ell^{1+\delta} \right).
\end{aligned}$$

Our above analysis, which is confirmed by the numerical experiments in Section 3, demonstrates that our importance sampling algorithm improves the strong convergence rate from $\beta = 1$ (see Figures 3.8 for Example 3.2, and 3.13 for Example 3.3) for the case without importance sampling, to $\beta = 1 + \delta$ with $\delta > 0$ (see Figures 3.11 and 3.12 for Example 3.2, and Figures 3.16 and 3.17 for Example 3.3) for the case with importance sampling. Due to Theorem 1.1, and given that $\gamma = 1$ for both cases, with and without importance sampling, we improve the complexity from $\mathcal{O}(TOL^{-2} \log(TOL)^2)$ for the case without importance sampling (since $\beta = \gamma$) to $\mathcal{O}(TOL^{-2})$ for the case with importance sampling (since $\beta > \gamma$), where TOL is a pre-selected tolerance.

3 Numerical Experiments

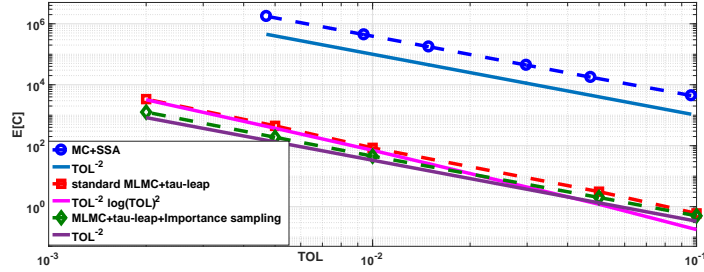
In the following, we illustrate the main benefits of our new proposed algorithm based on MLMC combined with importance sampling (explained in Section 2.2) compared to the standard MLMC as used in [3]. We consider three different examples of SRNs, given by Examples 3.1, 3.2, and 3.3, where we use the MLMC method to estimate $E[g(\mathbf{X}(T))]$, where \mathbf{X} is the state vector representing the counting number of each species in the system, $g: \mathbb{R}^d \rightarrow \mathbb{R}$ is a given smooth scalar observable of \mathbf{X} , and $T > 0$ is a user-selected final time. We show in Table 3.1 the summarized results, related to the convergence rates, for the different scenarios without/with importance sampling, and for the different examples that we consider in our numerical experiments. We also show different cases with respect to the parameter δ used in the importance sampling algorithm.

Example	α	β	γ	κ_L
Example 3.1 without importance sampling	1.06	1.06	1	2220
Example 3.1 with importance sampling ($\delta = 1/4$)	1.04	1.28	1	285
Example 3.1 with importance sampling ($\delta = 1/2$)	1.04	1.57	1	34.2
Example 3.1 with importance sampling ($\delta = 3/4$)	1.04	1.8	1	5.1
Example 3.2 without importance sampling	0.97	0.96	1	3170
Example 3.2 with importance sampling ($\delta = 1/4$)	0.98	1.21	1	386
Example 3.2 with importance sampling ($\delta = 1/2$)	1	1.47	1	51
Example 3.2 with importance sampling ($\delta = 3/4$)	1	1.72	1	5.83
Example 3.3 without importance sampling	1.02	1.03	1	1220
Example 3.3 with importance sampling ($\delta = 1/4$)	1.02	1.25	1	215
Example 3.3 with importance sampling ($\delta = 1/2$)	1.02	1.49	1	36.5
Example 3.3 with importance sampling ($\delta = 3/4$)	1.03	1.75	1	5.95

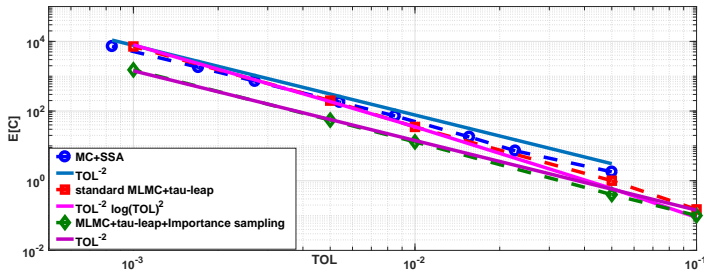
Table 3.1: Comparison of convergence rates (α, β, γ), and the kurtosis at the finest levels of MLMC, κ_L , for the different examples with and without the importance sampling algorithm. α, β, γ are the estimated rates of weak convergence, strong convergence and computational work, respectively, with a number of samples $M = 10^6$. The detailed convergence plots are presented below.

From this table, we can clearly see another advantage of our importance sampling algorithm besides dramatically reducing the kurtosis; we improve the strong convergence rates from 1 to $1 + \delta$, which, due to Theorem 1.1, improves the total complexity of the MLMC estimator from $\mathcal{O}(TOL^{-2} \log(TOL)^2)$ to $\mathcal{O}(TOL^{-2})$, where TOL is a pre-selected tolerance. This improvement

is confirmed by Figure 3.1, which shows that MLMC combined with our importance sampling algorithm achieves the same numerical complexity, $\mathcal{O}(TOL^{-2})$, as MC with an exact method (SSA), but with a significantly smaller constant. Furthermore, Figure 3.1 illustrates the improvement of the complexity rate compared to standard MLMC. For both examples 3.2 and 3.3, MLMC combined with the importance sampling algorithm significantly outperforms the standard MLMC. The detailed convergence plots for each example are presented below, obtained with a number of samples $M = 10^6$.



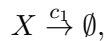
(a) Example 3.2.



(b) Example 3.3.

Figure 3.1: Comparison of the numerical complexity (expected work, $E[C]$, vs tolerance, TOL) of the different methods i) MC with SSA, ii) standard MLMC with TL, and iii) MLMC with TL combined with importance sampling ($\delta = \frac{1}{2}$). MLMC combined with our importance sampling algorithm achieves the same numerical complexity, $\mathcal{O}(TOL^{-2})$, as MC with an exact method (SSA), but with a significantly smaller constant. On the other hand, MLMC combined with importance sampling algorithm significantly outperforms standard MLMC.

Example 3.1 (Decay example). This model has one reaction,



with $c_1 = 1$, $T = 1$, and $X_0 = 10$. The stoichiometric scalar $\nu = -1$ and the propensity function $a(x) = c_1 x$. The quantity of interest in this example is $E[X(T)]$.

In Figure 3.2, we show the convergence plots for the MLMC method without importance sampling for Example 3.1. From this figure, and specifically from the right plot in the second row, we can see that for deep levels of MLMC, the kurtosis increases dramatically with respect to level ℓ of the MLMC method. This poor behavior of the kurtosis is mainly due to the *catastrophic coupling* issue (explained in Section 1.4.1), as illustrated by Figure 3.3.

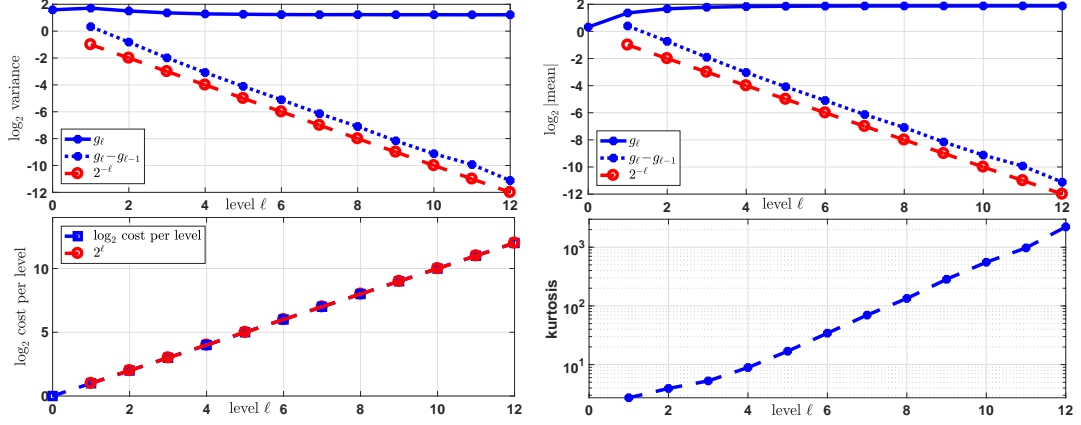


Figure 3.2: Convergence plots for MLMC without importance sampling applied to the decay example given by Example 3.1. $g_\ell = \overline{X}_\ell(T)$.

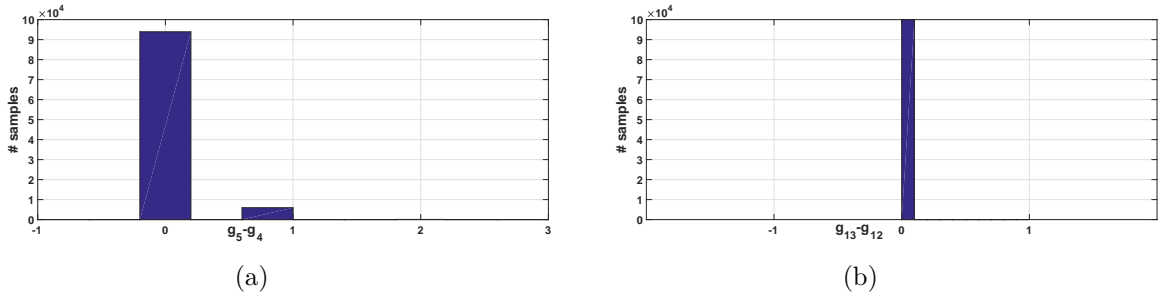


Figure 3.3: Histogram of $g_\ell - g_{\ell-1}$ ($g_\ell = \overline{X}_\ell(T)$) for the decay example without importance sampling, and for number of samples $M_\ell = 10^5$. a) $\ell = 5$. b) $\ell = 13$.

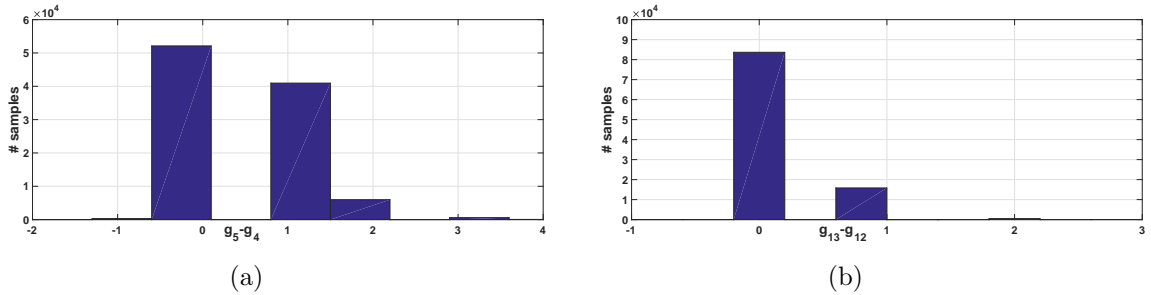


Figure 3.4: Histogram of $g_\ell - g_{\ell-1}$ ($g_\ell = \overline{X}_\ell(T)$) for the decay example with importance sampling with $\delta = \frac{3}{4}$, and for number of samples $M_\ell = 10^5$. a) $\ell = 5$. b) $\ell = 13$.

Using the MLMC estimator combined with importance sampling reduces the kurtosis significantly and improves the strong convergence rate from 1 to $1 + \delta$, as illustrated by Figures 3.5, 3.6, and 3.7 for $\delta = 1/4$, $\delta = 1/2$, $\delta = 3/4$, respectively. As shown from these plots, the optimal results are obtained for $\delta = 3/4$. The notable reduction of the kurtosis is mainly due to the signif-

icant reduction of the proportion of identical terminal values, g_ℓ and $g_{\ell-1}$, after using importance sampling, as can be seen from Figure 3.4.

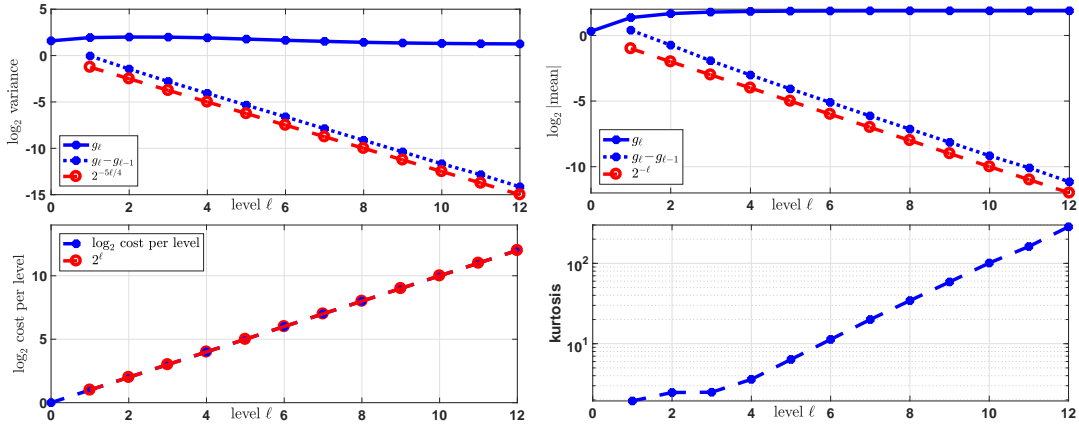


Figure 3.5: Convergence plots for the MLMC estimator combined with importance sampling with $\delta = 1/4$, for the decay example given by Example 3.1. $g_\ell = \overline{X}_\ell(T)$.

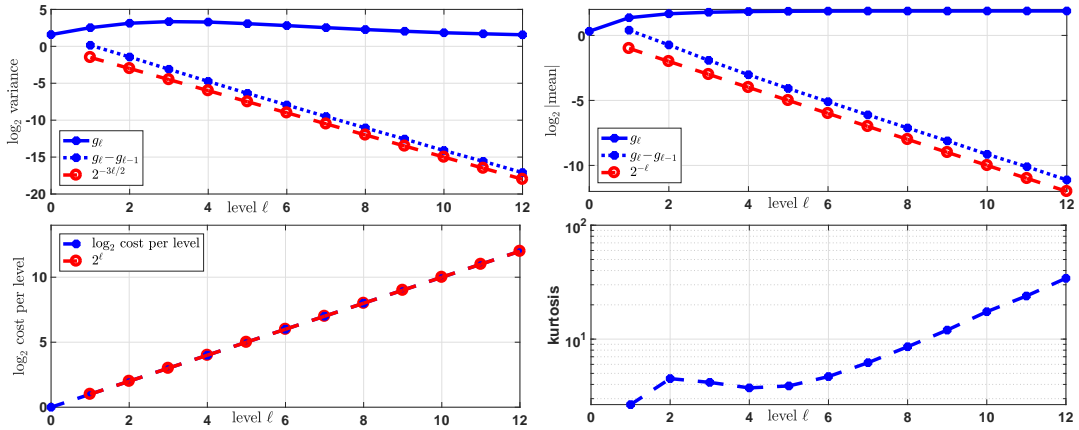


Figure 3.6: Convergence plots for the MLMC estimator combined with importance sampling with $\delta = 1/2$, for the decay example given by Example 3.1. $g_\ell = \overline{X}_\ell(T)$.

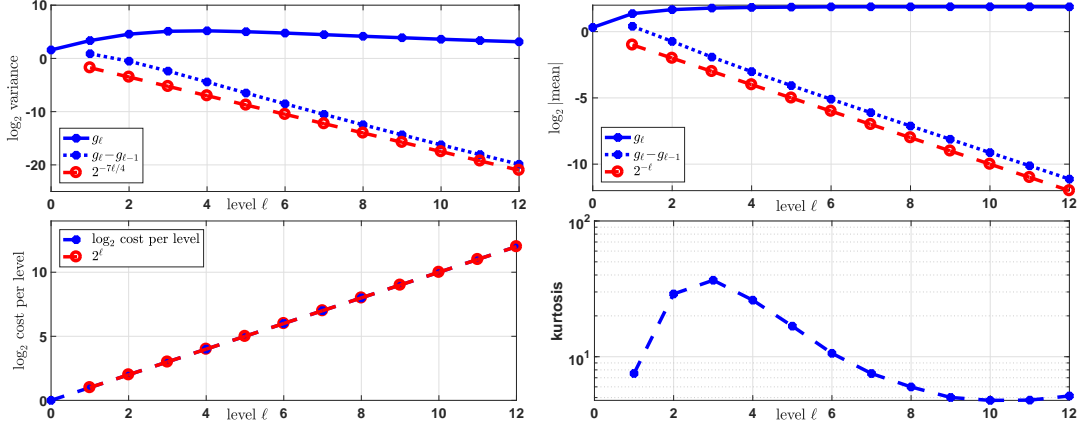
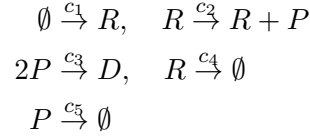


Figure 3.7: Convergence plots for the MLMC estimator combined with importance sampling with $\delta = 3/4$, for the decay example given by Example 3.1. $g_\ell = \overline{X}_\ell(T)$.

Example 3.2 (Gene transcription and translation [3]). This model has five reactions,



with $\mathbf{c} = (25, 10^3, 0.001, 0.1, 1)$, $T = 1$, $\mathbf{X}(t) = (R(t), P(t), D(t))$ and $\mathbf{X}_0 = (0, 0, 0)$. The stoichiometric matrix and the propensity functions are given by

$$\boldsymbol{\nu} = \begin{pmatrix} 1 & 0 & 0 \\ 0 & 1 & 0 \\ 0 & -2 & 1 \\ -1 & 0 & 0 \\ 0 & -1 & 0 \end{pmatrix}, \quad a(\mathbf{X}) = \begin{pmatrix} c_1 \\ c_2 R \\ c_3 P(P-1) \\ c_4 R \\ c_5 P \end{pmatrix}$$

The quantity of interest is $E[X^{(1)}(T)]$. We note that the choice of $X^{(1)}$ as the target species was determined by selecting the i th species with the highest probability of having $\overline{X}_\ell^{(i)}(T) - \overline{X}_{\ell-1}^{(i)}(T) = 0$, resulting in the most severe *catastrophic coupling* explained in Section 1.4.1.

In Figure 3.8, we show the convergence plots for the MLMC without importance sampling applied to Example 3.2. From this figure, and specifically from the right plot in the second row, we can see that for deep levels of MLMC, the kurtosis increases significantly with respect to level ℓ of the MLMC method. This poor behavior of the kurtosis is mainly due to the *catastrophic coupling* issue (explained in Section 1.4.1) as illustrated by Figure 3.9.

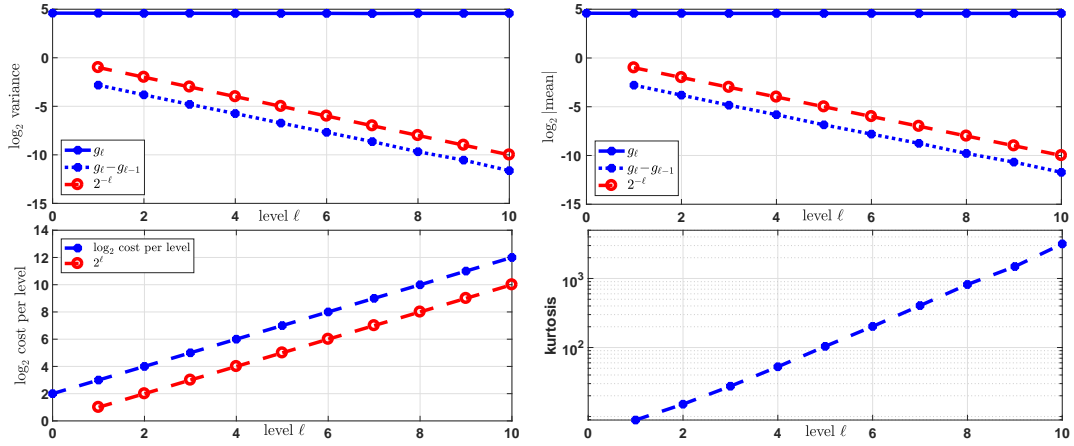


Figure 3.8: Convergence plots for MLMC applied to approximate $E[X^{(1)}(T)]$ for Example 3.2. $g_\ell = \overline{X}_\ell^{(1)}(T)$.

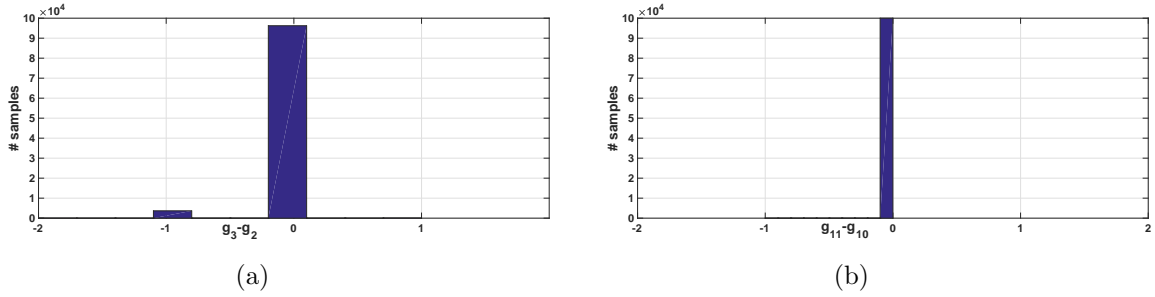


Figure 3.9: Histogram of $g_\ell - g_{\ell-1}$ ($g_\ell = \overline{X}_\ell^{(1)}(T)$) for Example 3.2 without importance sampling, and for number of samples $M_\ell = 10^5$. a) $\ell = 3$. b) $\ell = 11$.

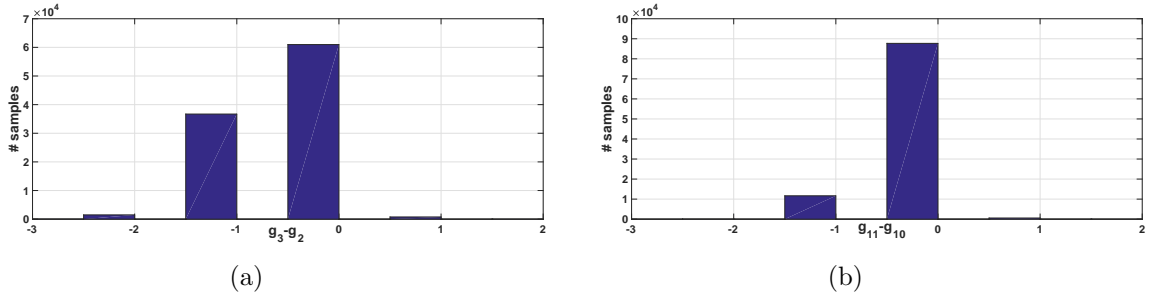


Figure 3.10: Histogram of $g_\ell - g_{\ell-1}$ ($g_\ell = \overline{X}_\ell^{(1)}(T)$) for Example 3.2 with importance sampling with $\delta = \frac{3}{4}$, and for number of samples $M_\ell = 10^5$. a) $\ell = 3$. b) $\ell = 11$.

Using the MLMC estimator combined with importance sampling reduces the kurtosis dramatically and improves the strong convergence rate from 1 to $1 + \delta$, as illustrated by Figures 3.11, 3.12 for $\delta = 1/2$, $\delta = 3/4$, respectively. As shown from these plots, the optimal results are obtained for

$\delta = 3/4$. The notable reduction of the kurtosis is mainly due to the significant reduction of the proportion of identical terminal values, g_ℓ and $g_{\ell-1}$, after using importance sampling, as can be seen from Figure 3.10.

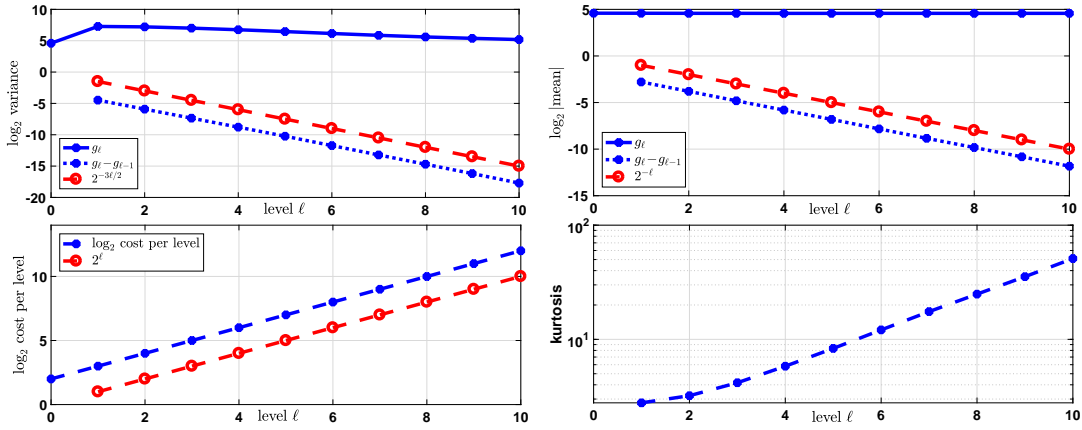


Figure 3.11: Convergence plots for the MLMC estimator combined with importance sampling with $\delta = 1/2$, to approximate $E[X^{(1)}(T)]$ for Example 3.2. $g_\ell = \overline{X}_\ell^{(1)}(T)$.

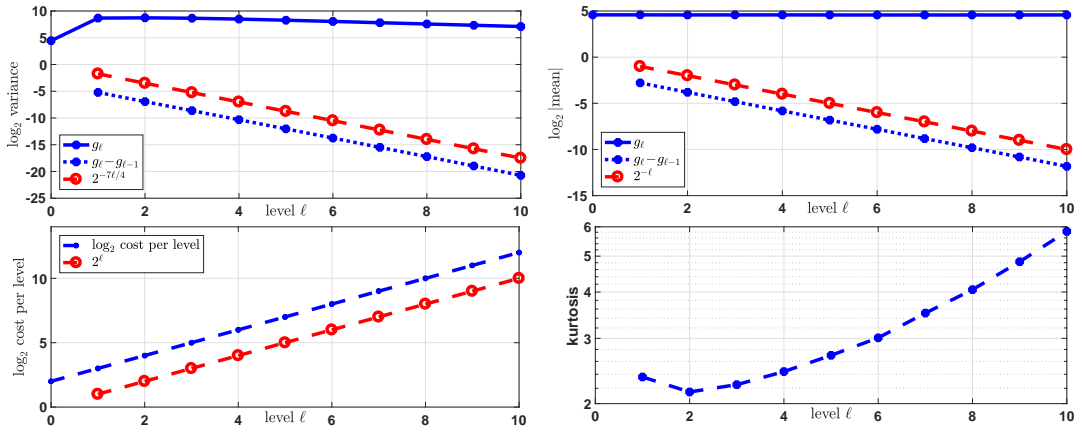
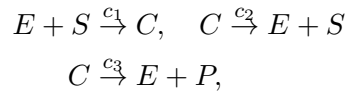


Figure 3.12: Convergence plots for the MLMC estimator combined with importance sampling with $\delta = 3/4$, to approximate $E[X^{(1)}(T)]$ for Example 3.2. $g_\ell = \overline{X}_\ell^{(1)}(T)$.

Example 3.3 (Michaelis-Menten enzyme kinetics [27]). The catalytic conversion of a substrate, S , into a product, P , via an enzymatic reaction involving enzyme, E . This is described by Michaelis-Menten enzyme kinetics with three reactions,



with $\mathbf{c} = (0.001, 0.005, 0.01)$, $T = 1$, $\mathbf{X}(t) = (E(t), S(t), C(t), P(t))$ and $\mathbf{X}_0 = (100, 100, 0, 0)$. The stoichiometric matrix and the propensity functions are given by

$$\nu = \begin{pmatrix} -1 & -1 & 1 & 0 \\ 1 & 1 & -1 & 0 \\ 1 & 0 & -1 & 1 \end{pmatrix}, \quad a(\mathbf{X}) = \begin{pmatrix} c_1 ES \\ c_2 C \\ c_3 C \end{pmatrix}$$

The quantity of interest in this example is $E[X^{(3)}(T)]$.

In Figure 3.13, we show the convergence plots for the MLMC method without importance sampling applied to Example 3.3. From this figure, and specifically from the right plot in the second row, we can see that for deep levels of MLMC, the kurtosis increases significantly with respect to level ℓ of the MLMC method. This poor behavior of the kurtosis is mainly due to the *catastrophic coupling* issue (explained in Section 1.4.1) as illustrated by Figure 3.14.

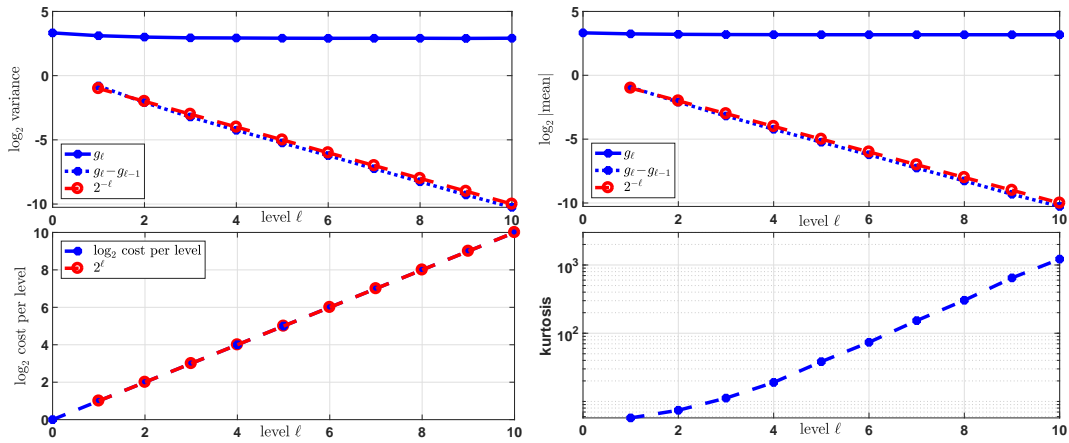


Figure 3.13: Convergence plots for MLMC applied to approximate $E[X^{(3)}(T)]$ for Example 3.3. $g_\ell = \overline{X}_\ell^{(3)}(T)$.

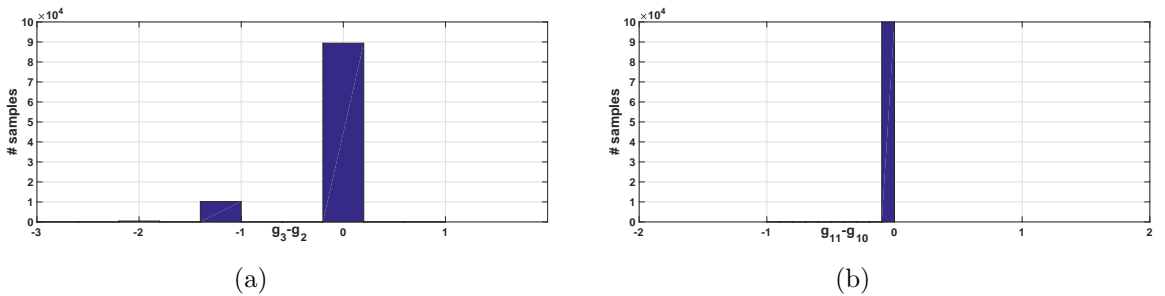


Figure 3.14: Histogram of $g_\ell - g_{\ell-1}$ ($g_\ell = \overline{X}_\ell^{(3)}(T)$) for Example 3.3 without importance sampling, and for number of samples $M_\ell = 10^5$. a) $\ell = 3$. b) $\ell = 11$.

Using the MLMC estimator combined with importance sampling reduces the kurtosis dramatically and improves the strong convergence rate from 1 to $1 + \delta$, as illustrated by Figures 3.16, and

3.17 for $\delta = 1/2$, $\delta = 3/4$, respectively. As shown from those plots, the optimal results are obtained for $\delta = 3/4$. The notable reduction of the kurtosis is mainly due to the significant reduction of the proportion of identical terminal values, g_ℓ and $g_{\ell-1}$, after using importance sampling, as can be seen from Figure 3.15.

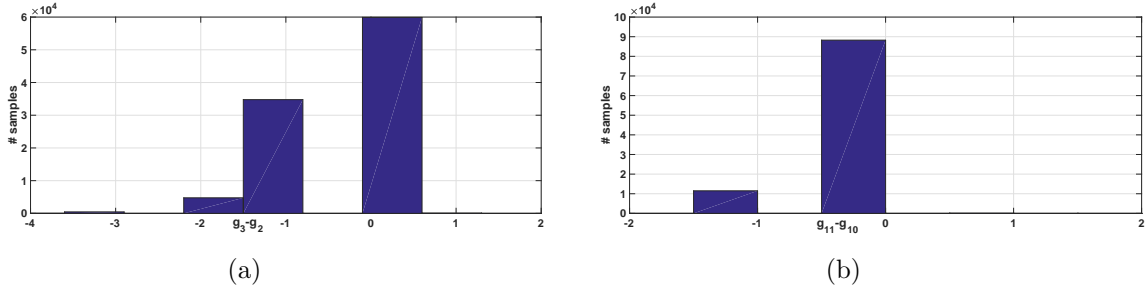


Figure 3.15: Histogram of $g_\ell - g_{\ell-1}$ ($g_\ell = \overline{X}_\ell^{(3)}(T)$) for Example 3.3 with importance sampling with $\delta = \frac{3}{4}$, and for number of samples $M_\ell = 10^5$. a) $\ell = 3$. b) $\ell = 11$.

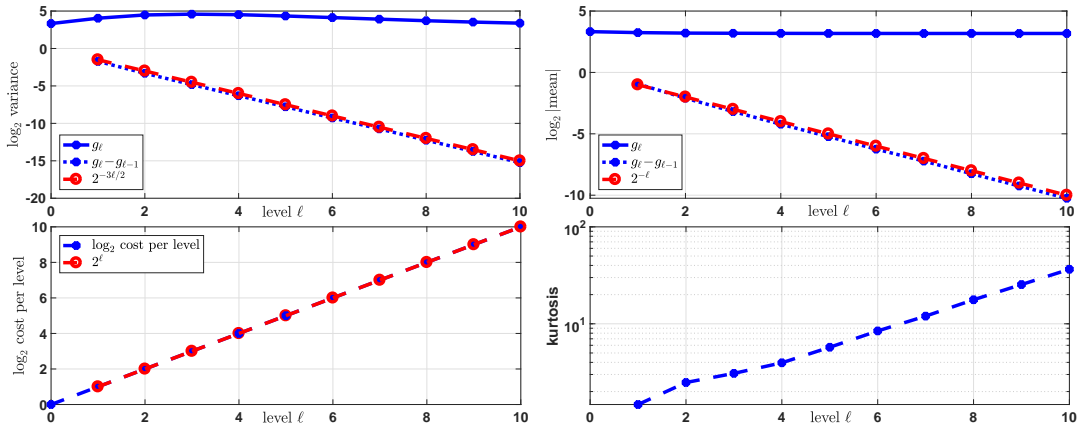


Figure 3.16: Convergence plots for the MLMC estimator combined with importance sampling with $\delta = 1/2$, to approximate $E[X^{(3)}(T)]$ for Example 3.3. $g_\ell = \overline{X}_\ell^{(3)}(T)$.

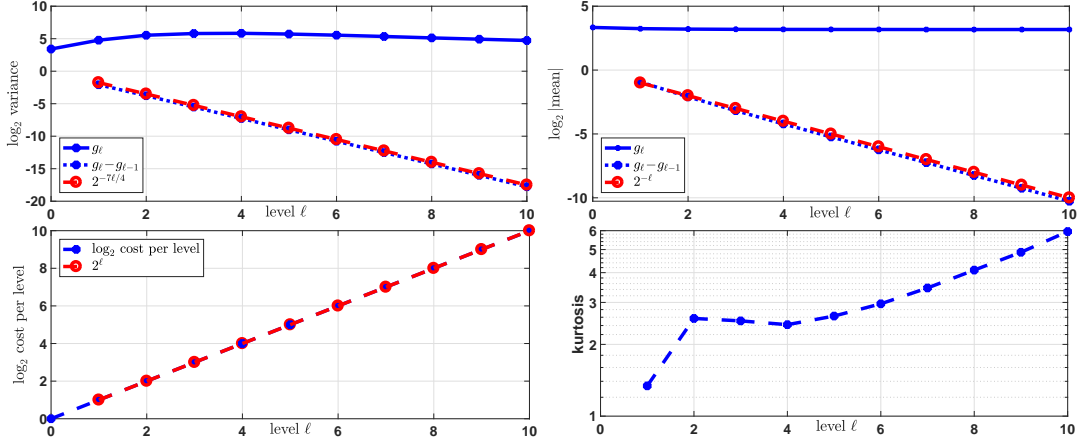


Figure 3.17: Convergence plots for the MLMC estimator combined with importance sampling with $\delta = 3/4$, to approximate $E[X^{(3)}(T)]$ for Example 3.3. $g_\ell = \overline{X}_\ell^{(3)}(T)$.

4 Conclusions and future work

In this work, we address the high kurtosis phenomenon related to catastrophic coupling in MLMC estimators of SRNs by proposing a novel path dependent importance sampling algorithm to be used with MLMC, to improve robustness and computational performance.

Our analysis and numerical experiments show that our proposed method not only increases the robustness of the multilevel estimator by dramatically reducing the kurtosis, but also improves the strong convergence rate, which results in improving the complexity of the MLMC method from $\mathcal{O}(TOL^{-2} \log(TOL)^2)$ to $\mathcal{O}(TOL^{-2})$, with TOL being a pre-selected tolerance.

In this work, we limited ourselves to using the importance sampling technique with an explicit TL scheme. In a future study, we intend to investigate the potential of our proposed algorithm when using a split step implicit TL scheme, as proposed in [19], which is required for systems with the presence of slow and fast timescales (stiff systems). To overcome the *catastrophic coupling* issue, the authors in [19] used extrapolation to get estimates for the sample variance when using MLMC. We believe our new importance sampling technique may help to achieve actual accurate estimates for sample variances needed for the MLMC estimator. Another potential research direction may investigate a more optimal importance sampling scheme to be used for MLMC; for instance, as discussed in Section 2.2, we may try to use a hierarchy of δ_ℓ , where the parameter δ used in our proposed method would depend on the level of discretization. Furthermore, we may explore the possibility of introducing a new importance sampling scheme for MLMC based on SPM coupling, to address the *catastrophic decoupling* issue, which is the second cause of the high kurtosis phenomenon in the context of SRNs when using MLMC. Finally, we can combine the strengths of our method and the hybrid approach as in [26] to improve the performance of the MLMC estimator.

Acknowledgments This work was supported by the KAUST Office of Sponsored Research (OSR) under Award No. URF/1/2584-01-01 and the Alexander von Humboldt Foundation. C. Ben Hammouda and R. Tempone are members of the KAUST SRI Center for Uncertainty Quantification in Computational Science and Engineering.

References Cited

- [1] Assyr Abdulle, Yucheng Hu, and Tiejun Li. Chebyshev methods with discrete noise: the τ -rock methods. *Journal of Computational Mathematics*, pages 195–217, 2010.
- [2] Tae-Hyuk Ahn, Adrian Sandu, and Xiaoying Han. Implicit simulation methods for stochastic chemical kinetics. *arXiv preprint arXiv:1303.3614*, 2013.
- [3] D. Anderson and D. Higham. Multilevel Monte Carlo for continuous Markov chains, with applications in biochemical kinetics. *SIAM Multiscale Model. Simul.*, 10(1), 2012.
- [4] David F Anderson. A modified next reaction method for simulating chemical systems with time dependent propensities and delays. *The Journal of chemical physics*, 127(21):214107, 2007.
- [5] David F Anderson and Thomas G Kurtz. *Stochastic analysis of biochemical systems*, volume 1. Springer, 2015.
- [6] Juan P Aparicio and Hernán G Solari. Population dynamics: Poisson approximation and its relation to the langevin process. *Physical Review Letters*, 86(18):4183, 2001.
- [7] Fred Brauer and Carlos Castillo-Chavez. *Mathematical models in population biology and epidemiology*, volume 40. Springer.
- [8] Yang Cao and Linda Petzold. Trapezoidal tau-leaping formula for the stochastic simulation of biochemical systems. *Proceedings of Foundations of Systems Biology in Engineering (FOSBE 2005)*, pages 149–152, 2005.
- [9] Erhan Çinlar. *Probability and stochastics*, volume 261. Springer Science & Business Media, 2011.
- [10] K Andrew Cliffe, Mike B Giles, Robert Scheichl, and Aretha L Teckentrup. Multilevel Monte Carlo methods and applications to elliptic PDEs with random coefficients. *Computing and Visualization in Science*, 14(1):3, 2011.
- [11] Darrell Duffie, Peter Glynn, et al. Efficient Monte Carlo simulation of security prices. *The Annals of Applied Probability*, 5(4):897–905, 1995.
- [12] Stefan Engblom. On the stability of stochastic jump kinetics. *arXiv preprint arXiv:1202.3892*, 2012.
- [13] Stewart N. Ethier and Thomas G. Kurtz. *Markov processes : characterization and convergence*. Wiley series in probability and mathematical statistics. J. Wiley & Sons, New York, Chichester, 1986.
- [14] Michael B Giles. Multilevel Monte Carlo path simulation. *Operations Research*, 56(3):607–617, 2008.
- [15] Michael B Giles. Multilevel Monte Carlo methods. *Acta Numerica*, 24:259–328, 2015.

- [16] Daniel T Gillespie. A general method for numerically simulating the stochastic time evolution of coupled chemical reactions. *Journal of computational physics*, 22(4):403–434, 1976.
- [17] Daniel T Gillespie. Approximate accelerated stochastic simulation of chemically reacting systems. *The Journal of Chemical Physics*, 115(4):1716–1733, 2001.
- [18] Ankit Gupta, Corentin Briat, and Mustafa Khammash. A scalable computational framework for establishing long-term behavior of stochastic reaction networks. *PLoS computational biology*, 10(6):e1003669, 2014.
- [19] Chiheb Ben Hammouda, Alvaro Moraes, and Raúl Tempone. Multilevel hybrid split-step implicit tau-leap. *Numerical Algorithms*, 74(2):527–560, 2017.
- [20] Sebastian C Hensel, James B Rawlings, and John Yin. Stochastic kinetic modeling of vesicular stomatitis virus intracellular growth. *Bulletin of mathematical biology*, 71(7):1671–1692, 2009.
- [21] Christopher Lester, Ruth E Baker, Michael B Giles, and Christian A Yates. Extending the multi-level method for the simulation of stochastic biological systems. *Bulletin of mathematical biology*, 78(8):1640–1677, 2016.
- [22] Christopher Lester, Christian A Yates, and Ruth E Baker. Robustly simulating biochemical reaction kinetics using multi-level Monte Carlo approaches. *Journal of Computational Physics*, 375:1401–1423, 2018.
- [23] Christopher Lester, Christian Adam Yates, Michael B Giles, and Ruth E Baker. An adaptive multi-level simulation algorithm for stochastic biological systems. *The Journal of chemical physics*, 142(2):01B612_1, 2015.
- [24] Tiejun Li. Analysis of explicit tau-leaping schemes for simulating chemically reacting systems. *Multiscale Modeling & Simulation*, 6(2):417–436, 2007.
- [25] Alvaro Moraes, Raúl Tempone, and Pedro Vilanova. A multilevel adaptive reaction-splitting simulation method for stochastic reaction networks. *SIAM Journal on Scientific Computing*, 38(4):A2091–A2117, 2016.
- [26] Alvaro Moraes, Raul Tempone, and Pedro Vilanova. Multilevel hybrid Chernoff tau-leap. *BIT Numerical Mathematics*, 56(1):189–239, 2016.
- [27] Christopher V Rao and Adam P Arkin. Stochastic chemical kinetics and the quasi-steady-state assumption: Application to the Gillespie algorithm. *The Journal of chemical physics*, 118(11):4999–5010, 2003.
- [28] Muruhan Rathinam. Moment growth bounds on continuous time Markov processes on non-negative integer lattices. *arXiv preprint arXiv:1304.5169*, 2013.
- [29] Muruhan Rathinam and Hana El Samad. Reversible-equivalent-monomolecular tau: A leaping method for small number and stiff stochastic chemical systems. *Journal of Computational Physics*, 224(2):897–923, 2007.
- [30] Ranjan Srivastava, L You, J Summers, and J Yin. Stochastic vs. deterministic modeling of intracellular viral kinetics. *Journal of theoretical biology*, 218(3):309–321, 2002.